Otto-von-Guericke University Magdeburg

Department of Computer Science

Master Thesis

Longitudinal MRI Image Processing and Classification of Rate of Brain Atrophy

Author:
Anshul Gupta

March 2, 2022

Advisors:

Prof. Dr. Christian Hansen
Otto-von-Guericke University
Faculty of Computer Science (FIN)
Universitätsplatz 2
39106 Magdeburg, Germany

Dr. Gabriel Ziegler
Otto-von-Guericke University
Faculty of Medicine University Hospital
Leipziger Str. 44
39106 Magdeburg, Germany

Gupta, Anshul:
Longitudinal MRI Image Processing and Classification of Rate of Brain Atrophy
Master Thesis, Otto-von-Guericke University
Magdeburg, 2022.

Abstract

Alzheimer's Disease (AD), characterized as a progressive neurological disorder, is often identified by the associated decline in cognitive functions such as forgetfulness or problems with language. Unfortunately, there is no cure; however, early detection can help deal with the associated effects of the disease. Detection of the disease is difficult due to overlapping features with aging; hence, precise detection and monitoring demand more sophisticated resources. This thesis work presents an automated method to detect patients with AD based on anatomical magnetic resonance imaging (MRI). Our method relies on using the segmented brain tissue, namely grey matter (GM), from the T1-weighted MRI scans from patients. A well-established support vector machines (SVMs) was applied to the segmented tissue to identify patterns that characterize clinical groups of AD. A real-world dataset from the DZNE DELCODE cohort with known class labels was used to build and evaluate the classification models. In particular, first, we build a baseline model that uses the cross-sectional MR data. Later, we model the structural changes in the brain over time using longitudinal MRI data. The longitudinal MRI scans were taken annually at three time points and rate of change images were obtained from these scans. We start by building a classifier to characterize subjects as healthy or cognitive decliners (subjective cognitive decline (SCD) or mild cognitive impairment (MCI)). Due to limited data over time, we have built a classifier to distinguish healthy subjects from MCI. The baseline model to classify unseen data as healthy and MCI obtained an accuracy of 75%, an F1 score of 74%, and an AUC score of 81%. While the longitudinal model attained an accuracy of 82%, an F1 score of 81%, and an AUC score of 82%. Additionally, the baseline model for classification of cognitive normal (CN), SCD, and MCI acquired an accuracy of 48%, an F1 score of 47%, and an AUC score of 63%. On the other hand, the longitudinal model outperformed the baseline model with an accuracy of 50%, an F1 score of 47%, and an AUC score of 65%. The overall performance of the SVM models based on longitudinal MRI data outperformed those built on cross-sectional MRI data.

Acknowledgements

I would like to thank Prof. Dr. Christian Hansen for giving me this opportunity to write this thesis. I am thankful for his support throughout the execution of this work.

I am very thankful for the support and guidance of Dr. Gabriel Ziegler in every step of this thesis work. Without his constant guidance, patience and encouragement this work could not have been possible. I express many thanks to Aditya Nemali who was always open for discussions, available for clearing my doubts and reviewing my work. I express my gratitude to Dr. Gabriel's team for giving me several opportunities to present my work, have open discussions and exchange ideas. I also thank Dr. Hartmut Schütze for helping me with network issues.

I am grateful of my friends, Srilekha Tummala and Simson Rodrigues for believing in my abilities and keeping me motivated. To my family, thank you for being there for me and always supporting me.

Contents

1 Introduction

The human brain is an organized network of billions of nerve cells termed as neurons. These neurons receive sensory input from external stimuli and send processed information to the muscles to perform any particular task. Precisely, the brain controls breathing, vision, arms, and legs movement, thoughts, emotions, memory, and several other processes that make our body functional [NOWINSKI (2011)]. In addition, our brain possesses extraordinary cognitive abilities that allow us to receive, select, store, transform, develop, and recover information from external stimuli [SQUIRE (2004)]. The brain helps us to effectively understand and relate to the external world [BRAUN (2008)]. Hence, even a minor disruption in the brain can drastically degrade the quality of life.

The brain is prone to various kinds of neurological disorders such as headache, seizures, stroke, epilepsy, including Alzheimer's Disease (AD) and Dementia [ORGANIZATION. (2006)]. Neurological disorders are often characterized by morphometric changes in the brain, which can be assessed using available brain imaging methods [WEINER und KHACHATURIAN (2005)]. Although locating the problem in the brain is critical because of its complex structure and overlapping features with aging, advanced imaging methods enable us to examine the morphological changes in the brain as a result of some injury, aging, or disease [HARDIMAN et al. (2011)].

AD is the most common cause of dementia, identified by a continuous and slow decline in thinking, social skills, and behavioral changes that can hurdle a person's ability to function independently. Some of the threatening effects of AD and dementia include the breakdown of neuronal connections, loss of synaptic efficiency, neuronal damage, and death, which in the final stages leads to macro-anatomical volume loss and is often called atrophy

[ROSEN et al. (2002)]. Progression towards AD typically begins decades before diagnosis, and the disease often gets unnoticed due to imperceptible associated symptoms. However, the early signs of cognitive impairment can be measurable in cognitive tests. In particular, Mild Cognitive Impairment (MCI) is marked as a transitional stage of AD, where people can no longer remember events that happened recently or the names of their family members. However, a person diagnosed with MCI can still function independently. Importantly, patients with MCI will not necessarily develop AD, but there is still a high risk of worsened effects with time [JACK JR et al. (2010)]. In the second stage of the disease, people may have trouble speaking, reading or writing, driving, forgetting where they live, and eventually wandering on the streets. Additionally, people with AD may get anxious and aggressive with time [THAKARE und PAWAR (2016)]. In the final stage of Alzheimer's, people may not recognize their close family members and require constant watch and care. AD usually commences after the age of 60, and the symptoms get worse with time [SAVVA et al. (2009)].

1.1 Motivation

It has been manifested that molecular proteomic changes and regional or whole-brain atrophy rate are strongly correlated with cognitive decline [FOX et al. (1999)]. Neurodegeneration, amyloid plaques, and neurofibrillary tangles are well-known associated hallmarks of progression towards AD. However, studies revealed that patients with amyloid do not necessarily develop significant clinical symptoms, neuronal and synaptic losses are the plausible determinants of cognitive decline in AD [JACK et al. (2008), JACK JR et al. (2010)]. Additionally, neuronal loss often leads to cerebral atrophy in certain brain areas such as the hippocampus located in the medial temporal lobe therefore, we can say that volumetric markers are often considered highly relevant for monitoring the disease progression towards AD [RUSINEK et al. (2003)]. It has been hypothesized by several research that AD occurs in two stages where amyloidosis and neuronal pathology (tauopathy, neuronal injury, and neurodegeneration) occur sequentially [MORMINO et al. (2009), DEKOSKY et al. (2002), TERRY et al. (1991)]. Furthermore, smaller regional volumes and larger ventricles can detect the development of AD, while there are reasons to believe that MCI might be detected by measuring minor volumetric changes in the same brain areas that later show substantial atrophy [DU et al. (2001)]. Since volume differences are not emphasized in earlier stages, the actual rate

of volume change might be informative. Moreover, hippocampal atrophy rate might best discriminate MCI subjects, whereas AD might be best identified from whole-brain atrophy, and regional measures of hippocampal atrophy are known to be the strongest predictors for progression of AD [HENNEMAN et al. (2009), LAAKSO et al. (2000), DE LEON et al. (1993), ERKINJUNTTI et al. (1993)]. Evidently, the microscopic changes in the brain may begin long before any symptoms appear therefore, it is reasonable to uncover early brain physiological changes using brain imaging methods [SCHOTT et al. (2005)]. Therefore, atrophy measured using structural magnetic resonance imaging (sMRI) is a powerful AD biomarker [FRISONI et al. (2010)].

Furthermore, results from observational surveys suggest that the aging of the world population can lead to an increasing number of adults with AD. The rise is expected to rocket from the current 26.6 million to 106.2 million by 2050 [BROOKMEYER et al. (2007)]. The disease is incurable at the moment however, diagnosis is an important step for studying disease-modifying factors such as behavioral interventions or drugs [DUNN et al. (2021)]. Early detection is important to run studies with novel disease modifiers. Early detection also provides an opportunity for patients and their family members to be prepared for the difficulties caused by the disease.

1.2 Objective

One of the most powerful methods for capturing essential macro-structural characteristics of the brain is magnetic resonance imaging (MRI). MRI Imaging is a non-invasive technique that provides the ability to capture positional data about the brain. It can potentially help to assess the disease-related changes in the brain. Additionally, repeated measures (or longitudinal) MRI of the brain can effectively help in tracking the progression of AD [RISACHER et al. (2010), RISACHER et al. (2009)]. Hence, the primarily goal of this thesis is to study the longitudinal changes in the brain caused by AD with the help of MRI scans of the patients tested at three annual follow-ups. In particular, the thesis aims to do the following - (1) cross-sectional and longitudinal image processing (segmentation and normalization), (2) adapting supervised learning frameworks for classification of MRI images, and (3) comparing the performance of cross-sectional and longitudinal MRI features on two classification tasks that distinguish disease stages. As a result, the thesis research questions can be described are as follows,

RQ1: How can we derive informative features (e.g., rate of change) from longitudinal MRI data that can provide potential biomarkers towards the progression of AD?

RQ2: How can we adapt our baseline (cross-sectional) classification algorithms to incorporate the features from longitudinal MRI data?

RQ3: Do longitudinal features offer improved performance for the classification of individuals during progression towards AD?

1.3 Contribution

The thesis is mainly focused on the longitudinal assessment of MRI images to track the progression of AD. Here, we use a supervised learning approach to detect different clinical groups involved at different stages of AD. In a nutshell, the contribution of this thesis can be summarized in the following,

- Firstly, we present binary and multi-class classification algorithms trained and evaluated on cross-sectional data. This methodology serves as the baseline approach for longitudinal assessment.
- The longitudinal studies enable assessment of the local rate of atrophy in various brain regions such as the hippocampus. Here, we derive atrophy rate images from longitudinal structural MRI processing using available pipelines characterizing brain changes using diffeomorphic deformations in a large sample of old age participants from the DZNE Delcode cohort (n=516, three scans per person, ages 60-90).
- We present binary and multi-class classification algorithms based on the above high-dimensional features to predict the diagnosis group involved in the progression of AD in terms of cognitive impairment over follow-ups.
- Finally, we aim to compare the classification performance of baseline and longitudinal models with the help of multiple metrics such as accuracy, F1 scores, and AUC scores. Additionally, we study and visualize the performance of proposed classification algorithms with the help of AUC-ROC curves.

1.4 Organization of the Thesis

The structure of the thesis is organised as follows,

- The subsequent chapter 2 gives the background about neuroscientific concepts that are integral to this thesis. Here, we have the description of AD and associated biomarkers, disease progression, available imaging techniques, and the role of machine learning algorithms in the detection of the disease through neuroimaging data analysis.
- In chapter 3, we review the literature of existing procedures and application of MRI data analysis. Here, we explore several existing applications of cross-sectional and longitudinal anatomical MRI scans in neuroimaging.
- Chapter 4 introduces the datasets used for this study, describes preprocessing of the MRI data, and details of the statistical analysis performed on the employed dataset. Moreover, this chapter includes the evaluation protocol, and opted metrics to quantify classification performance.
- Chapter 5 provides the outcome obtained from study. Here, we provide validation scores obtained from cross-validation, including accuracy, F1 score and AUC score for incorporated models. Additionally, test scores including identical metrics as validation for out-of-sample predictions on unseen data.
- Consequently, chapter 6 discusses the findings attained from the experiments of cross-sectional and longitudinal MRI data analysis.
- Chapter 7 concludes the thesis, and in this, we present conclusions based on the obtained results. This chapter also provides possible future work.

2
Background

This chapter provides the introduction and explanation of several concepts and techniques fundamental to this work. In section 2.1, we briefly explain the essential details about the complex brain structure and brain parts involved in cognitive functions. Subsequently, in section 2.2, we provide a detailed explanation of AD and associated anatomical changes in the brain. Here, we give a detailed explanation of involved biomarkers in AD, including amyloid plaques, neurofibrillary tangles, and brain atrophy. In the subsequent section 2.3, we discuss the progression of AD, including related symptoms and structural changes in the brain at different stages of the disease. Consequently, in section 2.4, we overview the scope of neuroimaging data in the detection and progression of Alzheimer's. Here, we further explain the selected types of neuroimaging techniques with some examples. Additionally, we look into the characteristics of neuroimaging data and available methods to extract and analyze the high-dimensional neuroimaging features. This thesis is primarily focused on analyzing structural changes associated with AD, therefore, in section 2.5, we give a detailed explanation about the neuroimaging technique explicitly used for this purpose. Finally, section 2.6 describes the classification and predictive modeling and introduces the proposed multi-class statistical model for this thesis work.

2.1 Brain Anatomy

The nervous system is consists of the brain, spinal cord, sensory organs, and billions of nerves that connect mentioned organs to the rest of the body. The brain is the most dominant organ in the human body, three critical parts include the cerebrum, cerebellum, and brain stem. The cerebrum occupies the

most space in the skull and is responsible for memory, reasoning, thoughts, vision, and emotions, including movement controls. The cerebrum's outer layer is called the cortex and plays a significant role in thinking ability. The cortex is comprised of millions of neurons arranged in specific layers. The nerve cell bodies appear to be grey-brown and, therefore, got the name grey matter (GM). Under the cortex are nerve fibers, also known as axons, that connect the brain areas called white matter (WM). The cerebellum is present at the back of the skull, underneath the cerebrum. The cerebellum controls muscle movements and postural adjustments to maintain balance. The third major part is the brainstem, which lies beneath the cerebrum in front of the cerebellum, which connects the brain to the spinal cord and controls breathing, heart rate, and blood pressure [FRACKOWIAK (2004)]. Additionally, Cerebrospinal Fluid (CSF) in the brain protects the brain tissues from external injury by providing a fluid buffer.

(a) human skull (b) a coronal slice

Figure 2.1: Example of a coronal slice of the brain containing GM, WM and CSF, adapted from [MedlinePlus]

2.2 Alzheimer's disease and associated biomarkers

AD is a progressive neurological disorder that eventually causes a gradual decline in cognitive functions. Anatomical changes in the brain can trace cognitive degeneration. Measures of such neurodegeneration are perhaps the most important biomarkers of AD [RASKIN et al. (2015)]. The associated biomarkers can be identified and tracked from the gross estimates of anatomical or neuropathological damage. Moreover, substantial evidence shows that volume differences can be closely related to AD and its variants [RISACHER et al.

(2009)]. AD is fatal as it can lead to the death of nerve cells and tissue loss throughout the brain [SMALE et al. (1995)]. An early symptom of AD is memory loss which destroys the parts of the brain involved in memory, including neurons and their connections, entorhinal cortex, and hippocampus. In addition, progressive loss of GM in AD patients causes a gradual thinning of the cortex. With time, the brain shrinks dramatically, affecting nearly all its functions and destroying the cerebral cortex [SHIN et al. (2005), TERRY et al. (1991)].

During the transition to AD, the brain goes through several molecular, cellular, and anatomical changes. Two molecular proteomic changes are characterized by two abnormalities in the brain: beta-amyloid plaques and neurofibrillary tangles (NFTs). Additionally, anatomical changes in the brain due to AD can also serve as important biomarkers that can be measured from anatomical neuroimaging techniques [JACK JR et al. (2010)]. The subsequent subsections describe these biomarkers associated with AD,

2.2.1 Amyloid Plaques

The beta-amyloid protein in AD patients comes in several molecular forms that accumulate between neuron connections. This protein is formed by breaking down a larger protein, known as the amyloid precursor. One of the most toxic forms of this protein is called beta-amyloid 42. An AD brain contains abnormal levels of these naturally occurring protein clumps, which eventually collects plaque between neuron connections causing a major disruption in cell functions [MAGALINGAM et al. (2018)]. In addition, proteins accumulate within the brain's GM while disrupting the brain's cognitive abilities. Therefore, researchers have been trying to better understand the formation and progression of this protein.

2.2.2 Neurofibrillary Tangles

This type of protein accumulates in the neurons of AD patients and is called tau. Microtubules, a support system for healthy neurons, carry molecules and nutrients from the cell body to the axons and dendrites. In a healthy subject, tau normally binds and stabilizes the microtubules. However, abnormal microscopic chemical changes in an AD subject break the connection between tau and microtubules and attach to other tau molecules. This variation in connections of tau leads to forming threads that can turn into tangles inside

neurons. These tangles hinder the communication between neurons while harming the synaptic transport system [BRAAK und BRAAK (1995)].

2.2.3 Brain Atrophy

Brain atrophy is characterized as macrostructural volume loss due to the loss of brain cells such as neurons. Brain cells can destroy the connection between neurons, hence impairing information processing and signal transmission. Brain atrophy is often closely related to cognitive decline, both cross-sectionally and longitudinally. This degeneration of brain cells often leads to several neurodegenerative disorders, including AD. Naturally, the aging process also causes the death of some brain cells, however, this process is slow and does not primarily affect neurons. In contrast, brain atrophy caused by disease or injury occurs more rapidly and can lead to lethal damage of neurons [PINI et al. (2016)].

Figure 2.2: Illustration of a healthy brain (left) vs. and brain of a patient diagnosed with AD (right), from BIRD (2008)

Moreover, these and other potential biomarkers of AD can be visualized with the help of Figure 2.3. It is expected first to observe a noticeable in proteomic/molecular biomarkers, followed by anatomical changes during the progression of AD [JACK et al. (2013)]. Finally, we observe a substantial rise in cognitive disabilities during the progression of the disease. Therefore, we can expect that associated biomarkers with AD might be used for staging and predicting progression towards AD. In particular, hippocampal atrophy has been known as an early hallmark of neurodegeneration in AD [BALL et al. (1985)].

Additionally, the volume reduction in the hippocampus is closely associated with cognitive decline [DE LEON et al. (1989)].

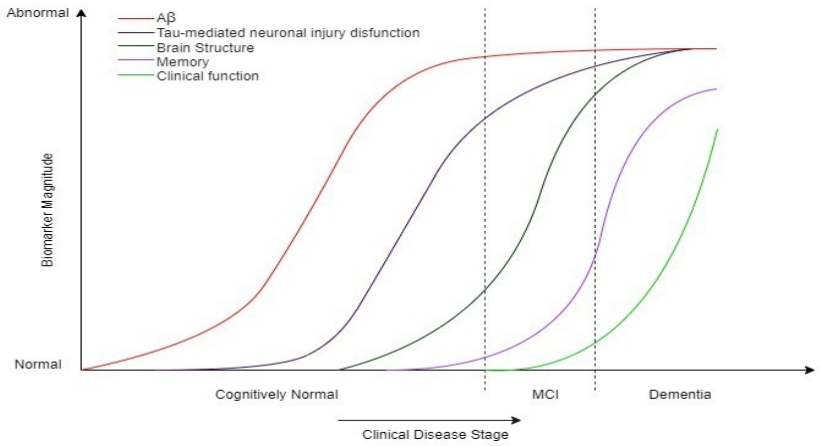

Figure 2.3: AD associated biomarkers as a function of disease progression, adapted from [JACK et al. (2013)]

2.3 Progression of Alzheimer's disease

Subtle neurodegeneration occurs early in AD development as we have seen that diffuse amyloid deposits contribute to neurodegeneration in the early stage of AD. However, neurofibrillary tangles have exhibited a characteristic pattern distribution that starts in the limbic system and, with time, progressively affects the neocortex. In general, there are five stages associated with AD: preclinical AD, MCI, mild dementia, moderate dementia, and severe dementia due to AD. Dementia causes a group of symptoms that affect intellectual and social abilities severely enough to degrade daily life function. In clinical contexts, the five stages can often not be differentiated, and instead, a 3 stage diagnosis system is used, including the preclinical stage, MCI, and the final AD stage [HANE et al. (2017b)]. The subsections will discuss clinical diagnostic stages involved in AD progression in more detail.

2.3.1 Preclinical Stage

Studies revealed that neurodegeneration due to AD might occur long before any symptoms appear [HANE et al. (2017a)]. Preclinical anatomical changes in

the brain, including amyloid buildups and alteration in other nerve cells, may be in progress already, however, there may be no significant clinical biomarkers of AD that can be traced yet [DUBOIS et al. (2016)]. This stage is called preclinical AD, can last for years, and is often get unnoticed by patients and their families due to unnoticeable symptoms.

2.3.2 Mild Cognitive Impairment (MCI)

Mild cognitive impairment (MCI) is marked by cognitive decline more than usual for a person's age and education level, however, these changes do not interfere notably with their daily life tasks. A person with MCI can find difficulty in remembering recent conversations, events, and appointments [GAUGLER et al. (2019)]. Empirical studies postulate that 3% to 19% of the population older than 65 years are affected by MCI. Although many individuals with MCI recover, more than half could progress to dementia in five years [GAUTHIER et al. (2006)]. Therefore, MCI is marked as a transitional risk stage, and early detection could help potentially prevent the risk factors.

2.3.3 Final Stage - Dementia

AD is often diagnosed at the mild dementia stage when the symptoms are significantly noticeable to doctors and family members. In this stage of AD, patients may have significant problems with memory and thinking abilities. Besides cognitive decline, a notable change occurs in the size of the brain and the accumulation of tau levels in the cerebrospinal fluid [SHARMA et al. (2021)]. Patients at this stage may find difficulty with problem-solving, face memory, and judgment lapses. Additionally, a patient at the mild dementia stage may go through some changes in personality such as anger, confusion, or low motivation. A patient at this stage may also find difficulty in organizing and expressing thoughts, or he may start to misplace belongings or himself. During moderate dementia caused by AD, the symptoms worsen, and the patient may need help with daily activities like bathing and self-care. Patients at this stage may also go through even more significant memory loss, including changes in personality and behavior. The last and most fatal stage of AD is severe dementia, which causes difficulty in communication, a decline in physical abilities like walking, eating, or even dressing. Muscles may become more rigid at this stage. Eventually, a patient loses the ability to swallow or control bladder func-

tions. The patient needs constant attention at this stage of the disease since it gets challenging to function independently [KALES et al. (2015)].

Furthermore, Figure 2.4 illustrates the decline in cognitive ability associated with different stages of AD. As we can observe, the cognitive decline at the preclinical stage is referred to as Subjective Cognitive Decline (SCD). If we notice, after SCD, the cognitive functions deteriorate swiftly with the progression of the disease.

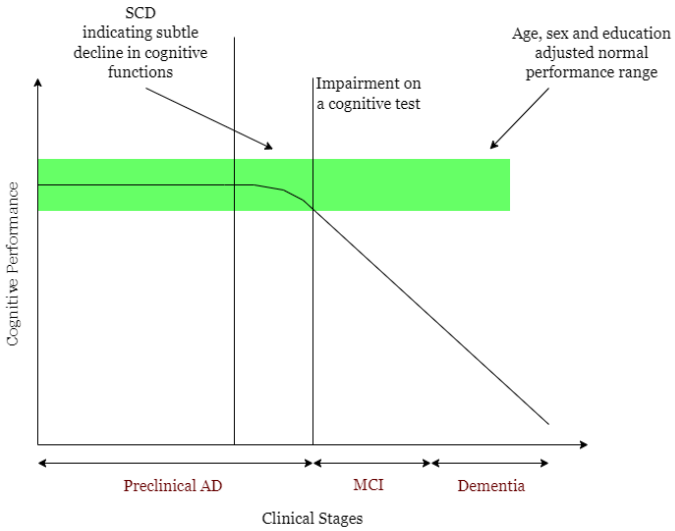

Figure 2.4: Course of cognitive decline with progression towards AD, adapted from [FOSTER et al. (2011)].

2.4 Neuroimaging Data and Analysis

Neuroimaging is a non-invasive method that captures structural, functional, and pathological features. Evidently, neurodegeneration is an integral part of AD, trauma, injury, and several other brain disorders, which can be analyzed with the help of neuroimaging [KLÖPPEL et al. (2012)]. Furthermore, atrophy and other significant biomarkers obtained from neuroimaging may significantly impact the diagnosis and prediction of the disease. Moreover, AD and other cognitively impaired patients are often tested routinely with different neuroimaging methods to detect and track the disease. Neuroimaging is widely categorized into structural and functional imaging.

- Structural imaging deals with the anatomical features of the brain, which can be used to diagnose tumors or even any injury in the brain. Structural imaging has revealed promising results in detecting different stages of AD, including dementia. Some common examples of structural imaging are computed tomography (CT) and structural magnetic resonance imaging (sMRI).

- Functional imaging is more restricted to diagnose metabolic diseases such as cortical dysplasia and cerebellar dysgenesis. This technique helps understand the activated parts of the brain with the help of blood flow while doing any particular cognitive activity, such as processing visual information or even lying [FLEISHER et al. (2005)]. Functional imaging includes positron emission tomography (PET) and functional MRI (fMRI).

Neuroimaging Data Analysis

Neuroimaging data is typically stored in 3D space while capturing the volumetric properties of different brain regions. Due to complex brain structures, neuroimaging data is typically extensive and complex. More specifically, the anatomical features of the brain are stored in 3D images with the recorder at every single point. The obtained data is measured in voxels, similar to pixels but in 3D. A standard example of an anatomical volume with an isotropic voxel resolution of 1mm comprises almost 17 million voxels, represented in a 3D matrix of 256 x 256 x 256 voxels.

Traditionally, neuroimaging data were analyzed by an experienced radiologist and involved manual measurements of characteristics of the brain. With advancements in technology, automated methods have been developed to assess the brain without the time-consuming manual measurements [OMBAO et al. (2016)]. One such automated technique is voxel-based morphometry (VBM), which has gained growing popularity due to its less complex and plausible findings [WHITWELL (2009), KLÖPPEL et al. (2008)]. VBM uses statistics to detect anatomical inhomogeneity in brains among groups of subjects. The findings in differences in brain regions can be exploited to identify brain atrophy in cognitively impaired patients. Typically, this technique uses volumetric MRI scans and performs statistical tests across all voxels in the MRI scans to detect regional anatomical or volumetric differences between subjects. This method has been widely used in a variety of studies, including neurodegeneration disorders [WHITWELL und JACK JR (2005)], mobility disorders [WHITWELL

und JOSEPHS (2007)], and epilepsy [KELLER und ROBERTS (2008)], while contributing to understand clinical biomarkers associated with neurological disorders.

2.5 Magnetic Resonance Imaging (MRI)

MRI is a powerful tool to capture exquisite details about the brain and has the advantage of visualizing the brain anatomy in all three planes: axial, sagittal, and coronal. In the simplest form, MRI techniques use the properties of the nuclear spin of protons in water molecules to create contrast in different brain tissues. It is based on the magnetization properties of the atomic water nuclei. An external strong uniform magnetic field is applied to align the protons within the examined tissue. This magnetization is then disrupted by another external Radio Frequency (RF) wave. The nuclei return to resting alignment through various relaxation procedures while emitting RF energy. Different kinds of images can be created by varying the sequence of RF pulses [MCROBBIE et al. (2017)]. The time between successive pulse sequences applied to the same slice is called Repetition Time (TR). Moreover, the time between the delivery of RF pulse and reception of the echo signal is termed as Time of Echo (TE).

2.5.1 MRI Imaging Sequences

Several sequences of RF waves and magnetic field gradients help to produce different types of images with different tissue contrasts. The three most common MRI sequences include T1-weighted, T2-weighted, and Flair scans. However, several other pulse sequences can also be employed to obtain brain scans. T1-weighted sequences are favored because they provide reasonable separation between GM, WM, and CSF intensities. On the other hand, T2-weighted images are preferred to detect brain lesions. The main difference between T1-weighted and T2-weighted images are the intensity distributions for several classes i.e. GM, WM and CSF. For T1-weighted images, the intensity of GM is more than that of CSF while WM is more intense than GM. In case of T2-weighted images, the order is just reversed [RISACHER et al. (2010)]. The MRI sequence produced at different settings can be summarized in following Table 2.1,

	T1_weighted	**T2_weighted**	**Flair**
Repetition Time (TR)	Short TR	Long TR	Very Long TR
Time of Echo (TE)	Short TE	Long TE	Very Long TE

Table 2.1: Common MRI imaging sequences with TR and TE times.

2.5.2 Structural MRI Imaging

MRI can measure brain morphometry at the macroscopic level. Therefore, it can capture GM atrophy caused by loss of brain cells, WM atrophy associated with loss in fiber connections, and expansion of CSF spaces. Particularly, structural MRI scans have proven potential significance in identifying biomarkers associated with many brain disorders, including MCI and AD, as well as in predicting the rate of progression of the disease [RISACHER und SAYKIN (2013), RISACHER et al. (2010)]. For example, studies have depicted that brain regions such as the medial temporal lobe tend to change during MCI and AD. Furthermore, these changes can be traced manually using regions of interest (ROIs).

Moreover, semi-automated tools such as voxel-based morphometry (VBM), tensor-based morphometry (TBM), and other related techniques can identify local and global tissue volume changes in MCI and AD subjects. Whole-brain, temporal lobe, and hippocampal GM density are significant biomarkers in MCI and AD subjects [RISACHER und SAYKIN (2011)].

Additionally, these and other associated biomarkers, such as cortical thickness, have been identified as potential biomarkers in predicting probable conversion of MCI to AD [JESSEN et al. (2014)]. The identified sensitive markers can be inferred from gross estimates of anatomical or neuropathological.

2.6 Classification Predictive Modeling

Characteristics molecular changes often precede the clinical presentation of the disease. Therefore, modeling approaches can predict clinical outcomes from MR-based neuroimaging markers. Classification is one such predictive modeling problem where the machine learning model will assign a class label to the unseen examples [QIU et al. (2017)]. The most straightforward classification predictive modeling problem will have examples belonging to only two classes, these problems are termed two-class classification or binary clas-

sification. On the other hand, when a classification predictive problem has data examples from more than two classes, such a task is termed a multi-class classification problem. This work has included binary and multi-class classification problems to identify the different diagnostic groups from healthy aging and AD populations.

3
Related Work

This chapter provides an overview of the state-of-the-art disease classification and progression modeling methods. The detailed information about existing research on statistical analysis of neuroimaging data is presented in subsequent section 3.1.

3.1 Literature Review

The growing interest in predictive modeling in medicine has attracted many researchers to employ machine learning algorithms to develop new diagnostic tools for diagnosis and clinical decision support [QIU et al. (2017)]. Advancements in statistical learning with improved machine learning algorithms enable the analysis of high-dimensional neuroimaging data. For instance, SVM does facilitate to development of novel diagnostic tools based on T1-weighted MRI [SCHÖLKOPF et al. (2001)]. Consequently, a vast range of approaches have been proposed to identify patients as AD and/or MCI from anatomical MRI scans [WEINTRAUB et al. (2012), COLLIOT et al. (2008), KLÖPPEL et al. (2008), CHUPIN et al. (2009), GERARDIN et al. (2009), MAGNIN et al. (2009), MISRA et al. (2009), QUERBES et al. (2009)]. These approaches have showed the potential to detect AD in the early stages. Based on the type of feature extraction method, these methods can be categorized into three groups, including voxel-based, vertex-based, or ROI-based. For this thesis work, we have used voxel-based method, which is the most common type of feature and it captures the sub-cortical GM areas such as the hippocampus. Several research works including [GOSCHE et al. (2002), VAN DE POL et al. (2006), LAAKSO et al. (2000), DE LEON et al. (1993), ERKINJUNTTI et al. (1993)] have supported that the rate of volume loss in medial temporal lobe and larger lat-

eral ventricles are potential diagnostic marker of AD. There is a vast amount of existing studies using voxel-based MRI [LAO et al. (2004a), FAN et al. (2008a), LAO et al. (2004b), KAUWE et al. (2010), MAGNIN et al. (2009)] and taking the advantage of SVMs to classify the brain images. Additionally, [ZHANG et al. (2014)] proposed a novel kernel SVM decision tree (kSVM-DT) method for classification of healthy, MCI and AD. The results show that the constructed kSVM-DT method attained a classification accuracy of 80%, while it was 74% without kernel.

Additionally, convolutional neural networks (CNNs) have been used widely for image data analysis due to their ability to process large unstructured data and automatically extract important features. Structural MRI-based CNN models for differentiating AD patients and healthy controls have been reported in numerous previous studies [BASAIA et al. (2019), LI et al. (2019), LI et al. (2018), LUO et al. (2017)]. Specifically, [JAIN et al. (2019)] has introduced a mathematical model PFSECTL based on transfer learning with a CNN architecture, VGG-16 trained on ImageNet dataset for feature extraction. And a 3-way classification is performed on the Alzheimer's Disease Neuroimaging Initiative (ADNI) database and obtained an accuracy score of 95.73% for the validation set. In addition, kernel methods have gained popularity in detecting patterns in unstructured high-dimensional data through transforming input space into a new features space. More details about kernels and their applications in machine learning can be found in [SHAWE-TAYLOR et al. (2004)].

Moreover, the disease is known to be common among the old-age population, and the detection can be optimized by identifying atrophy patterns in the brain more than expected for the age. Therefore, various studies [FRANKE et al. (2010), TIPPING (1999)] supported that accelerated aging is strongly related to accelerated brain atrophy. In order to recognize the brain atrophy from age, [FRANKE und GASER (2014)] introduced a framework for estimating the age from T1-weighted MRI scans using a relevance vector machine (RVM). Consequently, [FRANKE und GASER (2012)] presented a novel method that summarizes the complex, multidimensional aging pattern of the brain into a single value, the so-called BrainAGE score, which quantifies the acceleration or deceleration of individual brain aging. Evidently, age is an important factor in the detection of AD.

Also, the classification of MCI subjects from healthy controls has been explored by several studies, including [TEIPEL et al. (2007), DAVATZIKOS et al.

(2008)]. HUANG et al. (2010) and MESROB et al. (2009) use a different approach to group the voxels into anatomical regions through the registration of a labeled atlas. However, registration may not always adapt to the pathology. Therefore, to overcome this limitation [FAN et al. (2007)] suggested dividing the image space into most discriminative regions. This method was later adopted in several studies [FAN et al. (2008a), FAN et al. (2008b) and MISRA et al. (2009)].

4 Methods

In this chapter, we break down the task for this thesis work in terms of data description, preprocessing, and statistical analysis on the employed datasets. Firstly, section 4.1 provides the statistical information of the datasets used in this work. In particular, we provide a more specific description of the two kinds of datasets used in this study, including cross-sectional and longitudinal MRI data. Section 4.2 describes the preprocessing steps performed on the raw MR scans in order to extract meaningful high-dimensional features. Furthermore, section 4.4 introduces the SVM model and the specifications about its implementation for analyzing cross-sectional and longitudinal MRI data while incorporating the obtained features to predict and monitor the progression of the disease. In the following sections 4.4 and 4.5, we discuss the statistical analysis performed on both datasets, which aims to predict the clinical outcome of the participants using SVMs. Additionally, section 4.6 discusses the stratified k-fold cross-validation method that is commonly used to estimate the skill of machine learning algorithms. This popular statistical method is often employed in applied machine learning to compare and select a model for a specific predictive modeling problem. Subsequently, section 4.7 provides details about the experiment setup, and subsections introduce the metrics used to quantify the performance of the developed models.

4.1 Data Description

The dataset is obtained from the German Center for Neurodegenerative Diseases (DZNE) to build and evaluate the predictive models. In particular, DZNE has been conducting the multi-centric DZNE-Longitudinal Cognitive impairment and Dementia study (DELCODE), which involves participants belong-

ing to five discrete clinical groups, including subjects without cognitive symptoms (healthy control subjects) referred to as cognitive normal (CN), patients with Subjective Cognitive Decline (SCD), patients with Mild Cognitive Impairment (MCI) or dementia (AD), and first-degree relatives of patients with diagnosed AD (ADR). Since the disease is more common among old age people, the age of participants is often between 60 to 90 years.

4.1.1 Baseline MRI Data

The baseline MRI data includes 1079 subjects. These include 236 healthy controls (HC) without any cognitive impairment, 444 subjects with SCD, 191 cases with MCI, 126 AD, and 82 first-degree relatives of AD patients i.e., ADR [JACK et al. (2018)]. Out of 1079 subjects, T1-weighted MRI data was available for 975 subjects aged between 59 and 89 years old. Table 4.1 describes the summary of baseline MRI data.

	CN	SCD	MCI	AD	ADR
Sample size	230	392	165	110	76
Mean age(±SD)	69.4±5.4	71.3±6.1	72.9±5.6	75.2± 6.2	66.2± 4.5
Average education	14.7	14.8	14.0	12.8	14.6

Table 4.1: Summary of baseline MRI data, sample size represents the number of samples, age is in years, and the average education level of the participants.

4.1.2 Longitudinal MRI Data

The longitudinal MRI data from the DELCODE consists of 517 subjects with three T1- weighted MRI scans taken over annual time points. Sampling the same participant at different points gives freedom to track and predict the progression towards AD. The summary of the longitudinal MRI dataset is given in Table 4.2.

	CN	SCD	MCI	AD	ADR
Sample size	163	201	73	33	47
Mean age(±SD)	69.1±4.9	71.3±5.8	72.8±5.7	74.4± 6.8	66.2± 4.3
Average education	14.8	14.7	14.2	13.0	14.5

Table 4.2: Summary of longitudinal MRI dataset, sample size represents the number of samples, age is in years, and the average education level of the participants.

Furthermore, the DZNE cohort dataset was randomly split into training and test set in the ratio of 1:2, i.e., 66.66% of the total participants were involved in training. In contrast, 33.33% of the total participants were used for testing purpose only. Data partitioning is done while preserving the class distribution in both sets. The training set was solely used to train the proposed models and to cross-validate the classification performances. The test set was solely used to evaluate the classification performances of the employed models.

4.2 Data Preprocessing

Pre-processing is one of the important deciding factors in the performance of a machine learning algorithm. In the subsequent subsections, we briefly explain the details about preprocessing steps involved in this work. Firstly, we performed the segmentation of the MR scans belonging to three specific tissue types - GM, WM, and CSF. In particular, we have explored the GM tissue segment images for this thesis work, therefore, we have carried out further preprocessing only on those images. The second step involves the registration of GM images using diffeomorphic deformation. The obtained images from this step were smoothed to remove any unwanted noise. An Intracranial Volume (ICV) mask was used then to extract the regions of interest.

Additionally, the real-world dataset is prone to contain missing values, making it inconsistent and, therefore, degrading the performance of the machine learning algorithms. Therefore, we use a common technique to handle the missing values in the dataset, which includes simply dropping the null values. In this work, we have used the Pandas dropna function to remove the null values with their associated column or row from the data frame.

4.2.1 Segmentation

For the first step in preprocessing, we aim to fragment the original image into a set of non-overlapping semantically meaningful regions with similar attributes, including color, intensity, depth, or texture. The resulting image from segmentation can either be an image with labels identifying every homogeneous region or a contour image that describes the region boundaries.

The fundamental concept of MRI image segmentation is to classify the brain regions into specific tissue types and identify particular anatomical structures. For this work, we have segmented the MRI scans into three tissue types: GM,

WM, and CSF using the CAT12 segmentation toolbox [GASER et al. (2016)]. An example of tissue segmentation using CAT12 for T1-weighted MRI scan is illustrated in the following Figure 4.1.

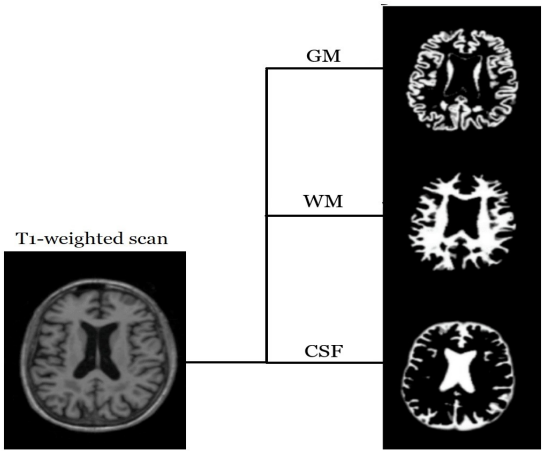

Figure 4.1: Brain tissue segments of T1-weighted scan obtained from CAT12.

4.2.2 Diffeomorphic image registration

The second step involved in preprocessing is image registration which aims to estimate a smooth and continuous mapping of the points in one image to the points in another image. A successful registration yields the relative shapes determined from the parameters that encoded the mapping. This step aims to determine the single 'best' set of values for these parameters. This algorithm is called DARTEL, standing for "Diffeomorphic Anatomical Registration Through Exponentiated Lie algebra" [ASHBURNER (2007)]. It can be used for both 2D and 3D image registration. The following Figure 4.2 illustrates an example of diffeomorphic registration for GM, WM and CSF volume segments obtained after different number of iterations.

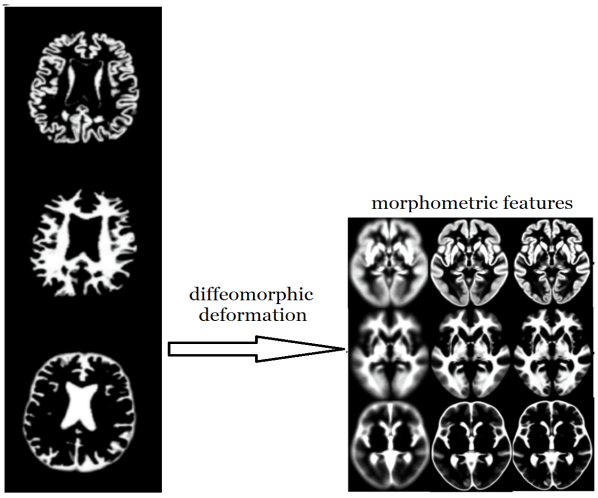

Figure 4.2: The figure shows the intensity averages of the GM (first row), WM (second row), and CSF (third row) images after different number of iterations.

4.2.3 Smoothing

Real-world data is often inconsistent and prone to noise. In particular medical data is generally inconsistent due to its high complexity or inaccuracy in measurement quality. Spatial smoothing was applied to the raw feature images to reduce the noise and gain detailed anatomical variability. The effect of smoothing was explored for varying degrees to find the optimum amount. The obtained raw features were smoothed for a range of 0mm to 20mm with an increment of 2-4mm using the full width at half maxima (FWHM) procedure.

4.2.4 Masking

Masking is a process of extracting specific voxels from the entire image. For example, masking can exclude non-brain voxels such as skull stripping or extracting the region-of-interest (ROI) from the entire original image. In this work, we have incorporated a predefined mask, the ICV mask, illustrated in Figure 4.3.

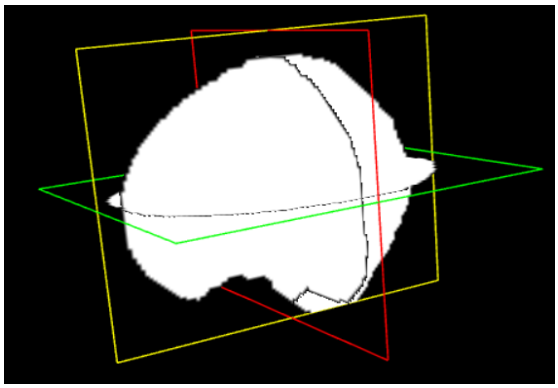

Figure 4.3: Illustration of ICV mask in 3D.

4.3 Support Vector Machines (SVMs)

A growing interest in neuroimaging field focuses on the exploitation of machine learning algorithms for deriving meaningful insights from the analysis of neuroimaging data. SVM is such supervised machine learning algorithm, introduced in 1995 [CORTES und VAPNIK (1995)] and widely used for both regression and classification tasks [MA und GUO (2014)]. SVM is more flexible and has a particular way of implementation when compared with other machine learning algorithms. SVM is known due to its ability to handle multiple continuous and categorical variables. For linearly separable data, the SVM algorithm aims to find a hyperplane in N-dimensional space that can distinctly separate the data points. Here, N represents the number of features, and support vectors are simply the coordinates of data points closer to the hyperplane, influencing most of the decision boundary.

Moreover, there can be several possible hyperplanes to separate the data points however, the SVM aims to search for a hyperplane that has the potential to maximize the margin, i.e., the maximum distance between data points from the involved classes. The dimensionality of the hyperplane highly depends on the number of features. Therefore, when the number of input features is two, the hyperplane will be a line as depicted in Figure 4.4, hyperplane dimensionality increases with an increase in the number of input features [XUE et al. (2009)].

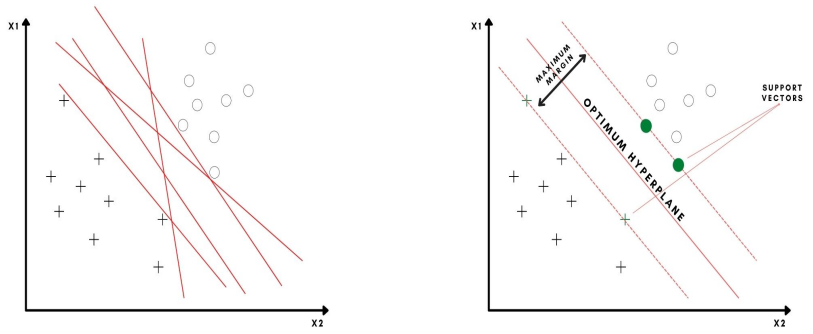

(a) Possible Hyperplanes (b) Maximum Margin Hyperplane

Figure 4.4: Illustration of possible hyperplanes and the optimum hyperplane with SVM.

Support vectors are another important contributor in deciding the position and orientation of the separating hyperplane. The support vectors are data points closest to the hyperplane that plays a major role in maximizing the margin. Maximizing the margin makes our solution more general, therefore, unseen data can be classified with more confidence. Therefore, we can define SVM as a discriminative supervised machine learning algorithm that outputs an optimal hyperplane that best categorizes the unseen future examples.

Kernel Function

SVM offers kernel functions to handle linearly inseparable data that transforms a low-dimensional input space into a higher-dimensional feature space. The kernel trick converts the non-separable problems into separable by adding more dimensions to the input space. Kernel trick makes SVM algorithm more versatile and powerful for prediction-based structural MRI analysis. Mathematically, for linearly inseparable data, SVM maps the data x in the input space I into a high dimension space H with a kernel function $\phi(x)$ as,

$$x \in \mathbb{R}^I \mapsto \Phi(x) \in \mathbb{R}^H \tag{4.1}$$

The kernel trick used by SVM is illustrated in Figure 4.5. As we can infer, the data points are linearly inseparable, therefore, SVM maps the input space to the feature space with the help of a kernel function and aims to find a hy-

perplane in higher-dimensional space in order to distinctly classify the data points.

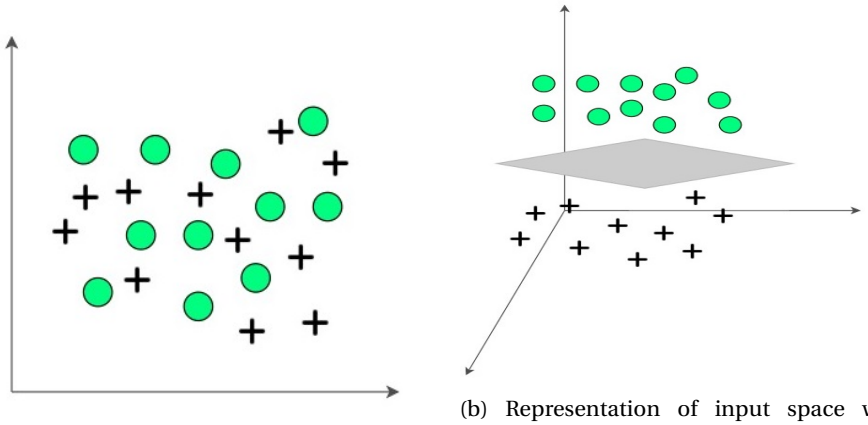

(a) Example of linearly inseparable data.

(b) Representation of input space when mapped to the feature space with the help of a kernel function.

Figure 4.5: Illustration of SVM kernel principle.

In this thesis work, we have incorporated linear kernels, which are the most basic kernels used by the SVM algorithm however, they are useful in the case of complex data. Linear kernel transforms the data from original input space to higher dimension space by calculating the dot product between two vectors, say x and x_i which is the sum of the multiplication of each pair of input values. The mathematical formulation of the linear kernel is given by,

$$\phi(x, x_i) = sum(x * x_i) \tag{4.2}$$

Initially, SVM was developed for binary classification problems only, however, it was later adapted for multi-class problems. SVM handles the multi-class problem by splitting it into multiple binary problems using the one-vs-one or one-vs-rest approach [HONG und CHO (2008)]. In this work, we have used the one-vs-rest approach, which trains SVM to distinguish a single class's data points from those of all other classes. While testing, the class label y of a class pattern x is determined by:

$$y = \begin{cases} n & \text{if } d_n(x) + th > 0 \\ 0 & \text{if } d_n(x) + th \leq 0 \end{cases} \tag{4.3}$$

where, d_n is $d_n(x) = max\{d_i(x)\}_{i=1}^{N}$, $d_i(x)$ represents the distance value from x to the SVM optimum hyperplane corresponding to class i and th is the classification threshold [YIN XIA et al. (2015)]. Furthermore, subsequent subsections provides the details about SVM specification and different settings used in this work.

4.3.1 Standard SVMs

In this study, we have developed a well-established SVM algorithm to accurately detect the presence of AD in a patient through the analysis of structural MRI data. The *sklearn* SVM model is employed with a linear kernel to handle the high-dimensional MRI features [PEDREGOSA et al. (2011)]. Here, a linear matrix is generated from the GM segmented images in practical terms. At this point, each MRI scan goes through a pair-wise multiplication with all other scans. Every element in the kernel matrix is simply a dot product of two MR scans. Intuitively, a kernel matrix can be seen as a similarity measure for the subjects assigned to a characterized group. The voxels in the MR scans are treated as coordinates of high dimensional space, and the intensity values determine their location at each voxel. The scans do not span the high-dimensional space but cluster in subspaces that accommodate only very similar scans.

4.3.2 Weighted SVMs

In order to handle the class imbalance in the incorporated datasets, we employ a weighted SVM where weights were assigned to distinct diagnosis groups. The weighted SVM learns the decision surface with respect to the relative influence of data points from each class. The *sklearn* SVM model is a powerful algorithm that can handle data imbalance with involved parameter *class_weight* [PEDREGOSA et al. (2011)]. The *class_weight* controls the value of another involved regularization parameter, C and set it to $class\_weight[i] * C$, where i represents the target class. The default value for *class_weight* is *None* which sets the weight for all the classes as one, hence treating all the classes the same. Conversely, when the value of the *class_weight* is set to *'balanced'*, the SVM model will set the weights to inverse of the class frequencies in the training data as $n\_samples/(n\_classes * np.bincount(y))$, where y represents the target class. The effect of weights on the decision bound-

ary can be seen in Figure 4.6, as we observe the decision boundary shifted towards majority samples when SVM sets the class weights.

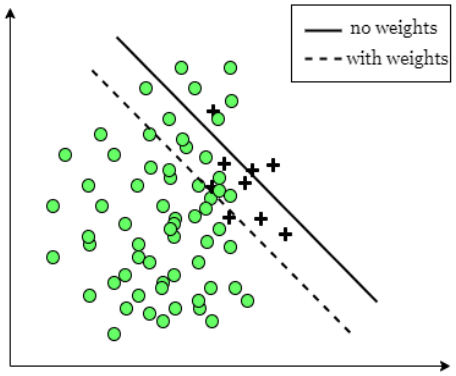

Figure 4.6: Illustration of shift in decision boundary with weighted SVM.

4.3.3 Multi-class SVMs

SVM handles the multi-class classification by fragmenting it into multiple binary classification problems. Two popular approaches are the One-vs-Rest and One-vs-One strategies. The first category, one-vs-rest splits the multi-class classification into one binary classification problem per class. In the second category, One-vs-One strategy breaks the multi-class classification problem into one binary classification problem for each pair of classes. For this thesis work, we have employed one-vs-rest, abbreviated as OvR and known as One-vs-All or OvA. Here, a binary classifier is trained on each binary classification problem, and a prediction is made with the most confident model. In case of multi-class problem, *sklearn* SVM offers involved parameter, $decision\_function\_shape$ which can be set to *'ovr'* to incorporate one-vs-rest strategy [PEDREGOSA et al. (2011)]. This parameter gives freedom to use binary SVM algorithms for multi-class problems.

Furthermore, the described SVMs are incorporated were trained on baseline and longitudinal MRI data for binary and multi-class classification tasks. The binary SVMs were designed to classify cognitively impaired patients from healthy controls. Additionally, we have extended the binary SVMs for the multi-class classification task. The SVM models were fit and cross-validated on training data using morphometric features extracted from GM volume segments. The goal of this work was to test the classification algorithms on

longitudinal MRI data, and the cross-sectional study has served as a baseline method. Moreover, the models were tested on an independent test set for evaluation purpose. The models were compared for individual studies as well as against each other for each study. In the following sections 4.4 and 4.5, we provide a detailed explanation of the application of the introduced SVMs for this work.

4.4 Application of SVMs to Baseline MRI data

Here, we have implemented the SVM model for cross-sectional MRI data, which has served as a baseline approach for our longitudinal analysis. In this case, 2mm resolution GM scans were used, and we acquired an optimum smoothing of 4mm with a Gaussian kernel. For our first study on baseline MRI data, we implement a binary SVM that aims to classify the participants as cognitively impaired and healthy. The primary aim of this study is to identify any abnormality caused by the disease in the brain by locating the biomarkers in the brain structure using GM segments. For our second study on the baseline MRI data, we executed a multi-class SVM to classify the baseline MRI data into three different diagnosis groups, including CN, SCD, and MCI. The description of the dataset used for this study with their target class labels can be inferred from Table 4.3 and Table 4.4. The test-train split was done while maintaining the target class distribution in both the sets. In the sub-sections, we have described further details for the binary model and the extended multi-class model which targets to differentiate the distinct the pathological stages involved in the progression of the disease.

4.4.1 Baseline Model - CN vs. MCI

As mentioned earlier, MCI causes cognitive decline more than expected for an individual's age or education level. The symptoms of MCI will not interfere noticeably with daily life activities, however, there is a high risk of the progress of this early stage to dementia over time. MCI is known to produce abnormal clumps of beta-amyloid protein identified as plaques. Moreover, brain MRI studies have shown associated changes with MCI, including shrinkage in the hippocampus and enlargement of ventricles [MORMINO et al. (2009)]. On the other hand, cognitively normal subjects are the healthy controls and do not show any abnormality in the brain's cognitive functions and responsible brain areas. For our first model, we have implemented a binary SVM model to

classify two selected clinical groups i.e., Cognitive Normal and Mild Cognitive Impairment. The class labels for the chosen groups are 0 and 1, respectively. The class distribution for this study can be referred from Table 4.3. The baseline models for binary classification include a standard SVM and a weighted SVM trained. These baseline SVMs were trained and tested on baseline MRI data. This study aims to identify even a anatomical disruption in a cognitively impaired brain.

Class Label	Description	Training	Test	Total
0	CN	154	76	230
1	MCI	110	55	165

Table 4.3: Class distribution in training and testing for binary classification problem using baseline MRI data.

4.4.2 Baseline Model - CN vs. SCD vs. MCI

Here, we have incorporated a third clinical group, SCD which served as a bridge between the preclinical stage to MCI and dementia. SCD occurs at the late stage of preclinical AD, characterized by a subtle decline in cognitive functions. Therefore, detection of SCD at an early stage can potentially contribute to the detection and diagnosis of AD. The description of the employed dataset is provided in Table 4.4. A standard SVM and a weighted SVM were trained and tested on baseline MRI data and the multi-class classification task was addressed using OvR strategy, where SVM fragments the multi-class problem into three binary classification problems defined as follows,

- **Binary Classifier 1:** CN vs. [MCI, SCD]
- **Binary Classifier 2:** MCI vs. [SCD, CN]
- **Binary Classifier 3:** SCD vs. [CN, MCI]

Class Label	Description	Training	Test	Total
0	CN	154	76	230
1	MCI	110	55	165
2	SCD	263	129	392

Table 4.4: Class distribution in training and testing for multi-class classification problem using baseline MRI data.

4.5 Application of SVMs to Longitudinal MRI data

Longitudinal studies allow researchers to study the local rate of atrophy in various regions of the brain [RISACHER et al. (2010)]. For this study, we derive the atrophy rates for longitudinal structural MRI images from the DZNE DELCODE cohort. Two available SPM pipelines with and without diffeomorphic deformations were used to pre-process the longitudinal features. Additionally, 12mm FWMH smoothing was used for denoising the images of rate of change of GM volume images. The test-train split was done while maintaining the target class distribution in both the sets. The primary aim of this study is to train and test our models on high-dimensional longitudinal features extracted from the images of rate of change of GM volume segments. We have explained the data description and model specifications for the longitudinal study in the following subsections.

4.5.1 Longitudinal Model - CN vs. MCI

A similar procedure like a baseline study for binary classification was used to classify subjects as CN and MCI. We have explored the different combinations of classes for binary study and compared the results. We have chosen to compare healthy patients against MCI instead of AD because of the scarcity of AD samples in the longitudinal MRI dataset. The first longitudinal model was designed to identify cognitively impaired patients from the healthy controls based on longitudinal MRI data. A linear kernel was used to address the high-dimensional MRI features. The following Table 4.5 summarizes the class distribution of data samples in training and test set.

Class Label	Description	Training	Test	Total
0	CN	109	54	163
1	MCI	49	24	73

Table 4.5: Class distribution in training and testing for binary classification problem using longitudinal MRI data.

4.5.2 Longitudinal Model - CN vs. SCD vs. MCI

We have extended the binary model to address the multi-class classification for longitudinal MRI data. In Table 4.6, we have described the details of the longitudinal MRI data used in this study. The multi-class problem was han-

dled in the same way as for baseline study i.e., by dissecting it into multiple binary classification problems using the OvR approach.

Class Label	Description	Training	Test	Total
0	CN	109	54	163
1	MCI	49	24	73
2	SCD	134	67	201

Table 4.6: Class distribution in training and testing for multi-class classification problem using longitudinal MRI data.

4.6 Model selection with stratified K-fold cross-validation

Cross-validation is a statistical resampling method to evaluate the generalization characteristic of a predictive model, it can also be used to prevent overfitting [T. HASTIE (2008)]. The basic idea of cross-validation is that the training and validation sets must cross over successively in a way that each sample has the opportunity to be validated against. The simplest form of cross-validation is known as k-fold cross-validation, where the data is split into k nearly equal folds, and k iterations of training and validation are performed. The algorithm uses a different fold for validation in each iteration, and k-1 folds are used for training purposes. In this work, we have employed a stratified five-fold cross-validation method which preserves a balanced class proportion in each fold. The general procedure of the employed method is illustrated in Figure 4.7. Only training data was used in cross-validation and the validation scores were calculated for each iteration, and an average of the values is then computed for five-folds in order to generalize the performance of the employed classification algorithms. Here, we have used validation accuracy, F1 scores, and AUC scores to quantify the classification performance of the SVMs on training data [PEDREGOSA et al. (2011)]. The description about the employed metrics is presented in following section 4.7.

Validate	Train	Train	Train	Train	Score - 1
Train	Validate	Train	Train	Train	Score - 2
Train	Train	Validate	Train	Train	Score - 3
Train	Train	Train	Validate	Train	Score - 4
Train	Train	Train	Train	Validate	Score - 5

Figure 4.7: Illustration of stratified five-fold cross-validation procedure.

4.7 Model Evaluation Protocol

Evaluation plays a crucial role in every machine learning pipeline. It is necessary to quantify the performance of a machine learning model to draw a meaningful conclusion. Several available metrics can be used to measure and monitor the performance of a machine learning algorithm during training and testing phase. In this work, we have addressed a binary and multi-class classification problems with discrete output using SVM models, therefore, we need a metric that compares discrete classes in some form. For this thesis work, we have tested our classification algorithms on an unused test set and calculated the accuracy, F1 scores, and AUC scores to quantify the classification performance of the SVMs [PEDREGOSA et al. (2011)].

Additionally, we have studied and visualized the performance using AUC-ROC curves, which are capable of summarizing the classification algorithms' performance at all possible threshold values. For binary classification, the ROC curves were plotted to analyse the performance of the employed classification algorithms on the test set. However, we have plotted ROC curves for each class in the case of multi-class classification in order to judge the performance of the model for every class. The following sections provide a description of the opted performance metrics and how we have incorporated these metrics for this thesis work.

4.7.1 Accuracy Score

Classification accuracy is perhaps the most used metric in machine learning. It is defined as a fraction of correct predictions [HANDELMAN et al. (2019)]. In particular, the accuracy is used to quantify the ability of a machine learning model to identify the relationships and patterns between variables in a dataset based on training data.

$$Accuracy = \frac{Numberofcorrectpredictions}{Totalnumberofpredictions} \tag{4.4}$$

The accuracy is favorable when the dataset is balanced i.e., an equal number of samples in each class, however, sometimes it can be misleading in the case of an imbalanced dataset. For example, consider that we have 98% of samples from class *A* and only 2% of the samples from class *B* in the training set, in this case, one can obtain a classification accuracy of 98% by predicting every unseen data sample as class *A*. In such a scenario, we might not be able to correctly evaluate the performance of our classifier, therefore, we have included the F1 score as well for a more precise evaluation.

4.7.2 F1 Score

Precision and recall are two essential model evaluation metrics. While precision refers to the percentage of relevant results, recall refers to the percentage of total relevant results that a machine learning algorithm has correctly classified. F1 score can be defined as the harmonic mean of precision and recall [HANDELMAN et al. (2019)]. It ranges between *0* and *1*, and a higher value means a better model. Mathematically, the F1 score can be represented by the following Formula 4.5.

$$F1Score = 2 * \frac{Precision * Recall}{Precision + Recall} \tag{4.5}$$

4.7.3 AUC-ROC Curve

To visualize and study the performance of our classification models, we use the AUC (Area Under The Curve) ROC (Receiver Operating Characteristics) curve. It is abbreviated as AUROC (Area Under the Receiver Operating Characteristics). It is one of the most valid evaluation metrics to evaluate a classification model's performance at various threshold settings [NARKHEDE (2018)].

ROC is a probability curve, and AUC defines the separability measure, i.e., how much the classification model can distinguish between target classes. The value of AUC directly influences the performance, therefore, the higher the AUC, the better the model in distinguishing between the classes. The AUROC plots the True Positive Rate (TPR) against False Positive Rate (FPR), where TPR lies on the y-axis while FPR is on the x-axis.

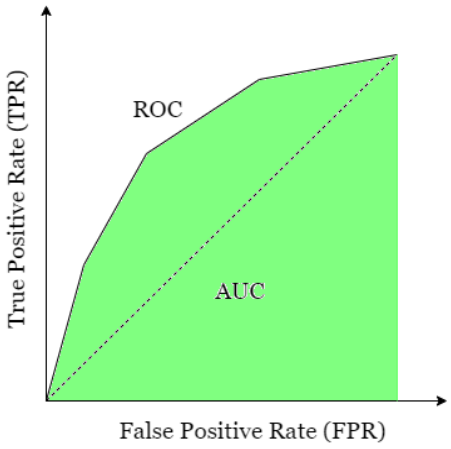

Figure 4.8: AUC-ROC Curve Illustration

5 Results

For this work, we have developed and evaluated the SVM models for two different kinds of data, including baseline and longitudinal MRI data. The prprocessing is performed as mentioned in Chapter 4, section 4.2. The MRI scans were segmented with CAT12, and GM, WM and CSF volume images were obtained, we have used only T1-weighted GM scans for further analysis. DARTEL algorithm was used for image registration. The optimum smoothing obtained for baseline data was 4mm on 2mm resolution images. In contrast, in the case of longitudinal data, a more intense smoothing is applied with 12mm. Finally, an ICV mask was employed to extract the region of interest. Furthermore, we have performed several statistical analyses on both the datasets as described in previous chapter 4, section 4.4 and 4.5. Specifically, we have presented a standard SVM model with a linear kernel to address the classification problems, which include binary as well multi-class classification tasks. Moreover, to address the class imbalance in the incorporated datasets, we have used a weighted SVM model which targets to set a predefined weight to each data point from all the classes.

In this chapter, we have presented the classification performance of each model using accuracy, F1 score and AOC score averaged on five folds of cross-validation as mentioned in chapter 4, section 4.6. The validation scores are capable to generalize the classification performance of the models while allowing every data instance to take part in training the classifiers. Additionally, we have visualized the performance using AUC-ROC curves, summarizing the classification algorithms' performance at all possible threshold values. And the ROC curves were also plotted to illustrate the performance of our classification algorithms on the test set.

5.1 Baseline Models

5.1.1 Classification of CN vs. MCI

For our first SVM model, we have done the binary classification for healthy vs. cognitively impaired patients, i.e. CN vs. MCI. Here, we have trained our SVM model with a linear kernel to handle the high-dimensional GM scan data. Additionally, we have employed a balanced SVM, where SVM is assigning weights to each data point as described in the chapter 4, section 4.4. The primary aim of this study is to find any discernible patterns in the brain structure caused by the disease.

Validation Scores

For model selection, we have used the stratified five-fold cross-validation method. Table 5.1 summarizes the validation scores averaged on five-folds for our binary classification algorithm for baseline data analysis. Here, we aim to compare the classification performance of SVMs with the help of accuracy, F1 score and AOC score.

Model	Accuracy	F1 Score	AUC Score
standard_SVM	0.74	0.72	0.80
weighted_SVM	0.76	0.73	0.81

Table 5.1: Comparison of averaged accuracy, F1 score, and AUC score obtained from stratified five-fold cross-validation for binary classification using the standard and the weighted SVM algorithms.

Test Scores

The SVM models were tested on an unused test set to classify the subjects into different clinical groups. Here, we aim to compare the performance of the models on unseen data with the help of accuracy and F1 score. Table 5.2 summarizes the results obtained from this study. Additionally, we have plotted the ROC curves to compare the performance of standard SVM and weighted SVM in Figure 5.1 and computed the AUC scores. We also compute the optimum thresholds for each classifier.

Model	Accuracy	F1 Score
standard_SVM	0.75	0.74
weighted_SVM	0.75	0.74

Table 5.2: Comparison of test accuracy and F1 score for binary classification of baseline data using the standard SVM and weighted SVM model.

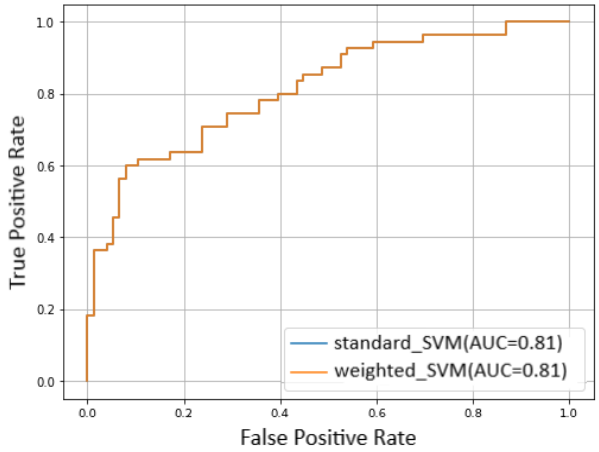

Figure 5.1: Illustration of binary classification performance of the standard and the weighted SVM model on test set for baseline data analysis.

5.1.2 Classification of CN vs. SCD vs. MCI

As we have discussed in Chapter 4, Section 4.3.3, the SVM model can be extended for multi-class classification problems using the one-vs-rest approach. Here, we present the multi-class classification performance of standard SVM and weighted SVM that aim to identify the clinical stages involved in AD, i.e. CN, SCD, and MCI. GM volume segments were used to train and test the models. The SVM models are applied with a linear kernel to handle the high-dimensional features. The aim of this study was to detect the progression of AD by detecting the different clinical stages involved in the progression of the disease.

Validation Scores

Table 5.3 summarizes the classification performance of the standard SVM and the weighted SVM model for multi-class classification problem. As we have

mentioned earlier that validation scores are averaged on five-folds, which gives us the freedom to judge the general performance of our classifiers.

Model	Accuracy	F1 Score	AUC Score
standard_SVM	0.46	0.38	0.64
weighted_SVM	0.48	0.42	0.65

Table 5.3: Comparison of averaged validation accuracy, F1 score, and AUC score in five-folds for multi-class classification of baseline data, using the standard SVM and the weighted SVM models.

Test Scores

The classification algorithms used for this thesis work, i.e. standard SVM and weighted SVM, were tested on an unseen dataset, and the accuracy and F1 scores were calculated for each model. Table 5.4 summarizes the classification performance of the used models for multi-class classification with employed metrics. Additionally, Figure 5.2 and Figure 5.3 illustrate the summary of the classification performance ROC curves for each class, and a macro-averaged ROC curve computes an average performance on each class without considering any heuristic i.e., treating every class equal. We have obtained similar ROC curves for both the classifiers therefore, we have titled the figures to discriminate the results for our classifiers in this case.

Model	Accuracy	F1 Score
standard_SVM	0.48	0.47
weighted_SVM	0.48	0.47

Table 5.4: Comparison of test accuracy and F1 score for multi-class classification of baseline data using the standard SVM and weighted SVM model.

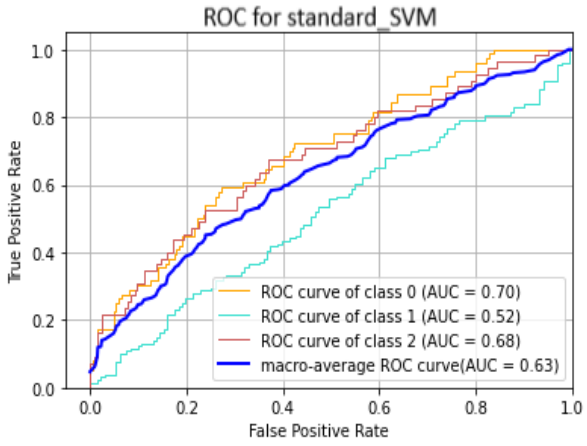

Figure 5.2: Illustration of performance of the standard SVM algorithm for multi-class classification of baseline MRI data using ROC curves for individual classes. The blue solid curve represents the macro-average ROC curve on all three classes.

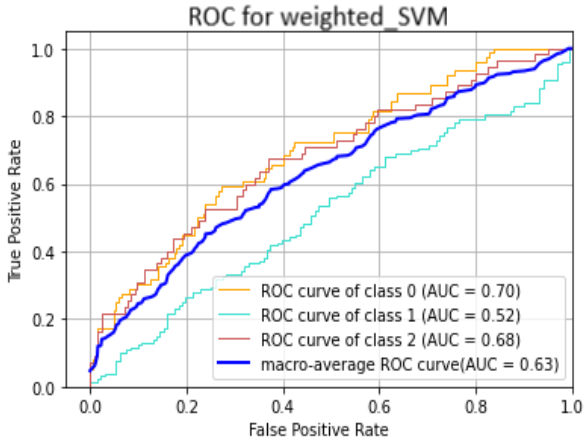

Figure 5.3: Illustration of performance of the weighted SVM algorithm for multi-class classification of baseline MRI data using ROC curves for individual classes. The blue solid curve represents the macro-average ROC curve on all three classes.

5.2 Longitudinal Models

The participants for longitudinal analysis were tested annually at three-time points, and the linear rate of change images were derived from these scans for

each participant. The pre-processing steps, as described in the previous chapter 4, were performed, and the linear rate of change images for GM segments were obtained with the help of the voxel-wise ridge regression technique. In the subsequent subsections, we have provided the findings for both binary and multi-class classification problems.

5.2.1 Classification of CN vs. MCI

For the binary classification problem, we aimed to classify healthy from the cognitively impaired patients with the target class labels as CN and MCI. The validation scores were average on five-folds. Similar to baseline analysis, the SVM models are applied to longitudinal data, and classification performance is judged based on accuracy, F1 score, and AUC score. Here, we finally aimed to compare the performance of SVM models for both the studies, i.e. baseline and longitudinal.

Validation Scores

The validation scores for standard SVM and weighted SVM, which include average accuracy, F1 score, and AUC score on five-folds are specified in Table 5.5. The aim of this study is to detect any anomaly in the brain structure caused by the disease.

Model	Accuracy	F1 Score	AUC Score
standard_SVM	0.75	0.65	0.70
weighted_SVM	0.77	0.69	0.72

Table 5.5: Comparison of averaged validation accuracy, F1 score, and AUC score in five-folds for binary classification of longitudinal data, using the standard SVM and the weighted SVM models.

Test Scores

The classification performance of the standard SVM and weighted SVM were evaluated on unseen data. Table 5.6 compares the classification performance of the proposed models with the help of test accuracy and F1 score. Moreover, the performance of the classification algorithms were illustrated with ROC curves plotted in Figure 5.4. In addition, we have calculated the optimum threshold for the incorporated models.

Model	Accuracy	F1 Score
standard_SVM	0.82	0.81
weighted_SVM	0.82	0.81

Table 5.6: Comparison of test accuracy and F1 score for binary classification of longitudinal data using the standard SVM and weighted SVM model.

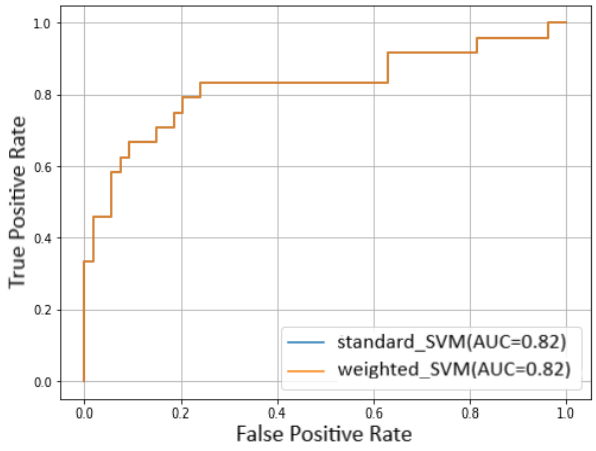

Figure 5.4: Illustration of binary classification performance of the standard and the weighted SVM algorithms on the test set for longitudinal data analysis.

5.2.2 Classification of CN vs. SCD vs. MCI

A similar set of classes as baseline were used for multi-class classification of longitudinal data. Here, we have included three clinical groups while aiming to detect the progression of the disease.

Validation Scores

As mentioned before, validation scores were averaged on five-folds to generalize the performance of the classifiers. We can compare the classification performance of the SVM models with validation scores for multi-class classification as presented in Table 5.7.

Model	Accuracy Score	F1 Score	AUC Score
standard_SVM	0.50	0.38	0.65
weighted_SVM	0.55	0.48	0.66

Table 5.7: Comparison of averaged validation accuracy, F1 score, and AUC score in five-folds for multi-class classification of longitudinal data, using the standard SVM and the weighted SVM models.

Test Scores

The evaluation of the presented classification algorithms was done on an independent dataset referred to as an test set. The classification scores were calculated with the help of accuracy and F1 score, as given in Table 5.8. Additionally, ROC curves were plotted for each model, as shown in Figure 5.5 and Figure 5.6. The performance of the classifiers was tested on individual classes, and a macro-average ROC curve was plotted to generalize the performance of the models on all included classes.

Model	Accuracy	F1 Score
standard_SVM	0.47	0.46
weighted_SVM	0.50	0.47

Table 5.8: Comparison of test accuracy and F1 score for multi-class classification of longitudinal data using the standard SVM and weighted SVM model.

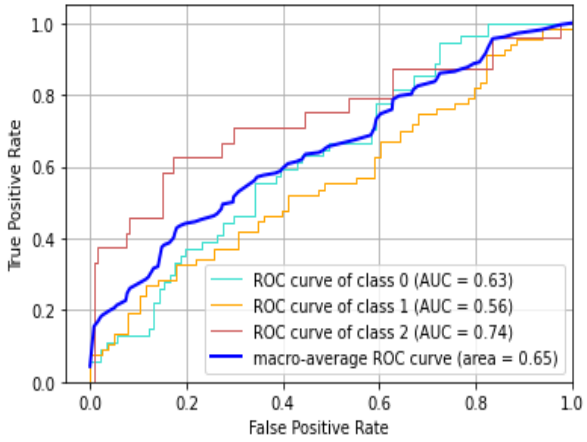

Figure 5.5: Illustration of performance of the standard SVM algorithm for multi-class classification of longitudinal MRI data using ROC curves for individual classes. The blue solid curve represents the macro-average ROC curve on all three classes.

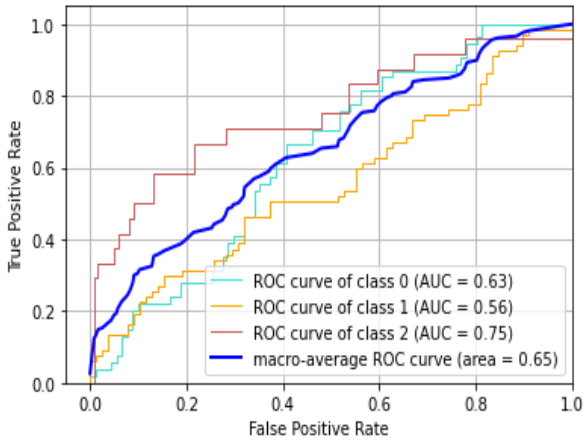

Figure 5.6: Illustration of performance of the weighted SVM algorithm for multi-class classification of longitudinal MRI data using ROC curves for individual classes. The blue solid curve represents the macro-average ROC curve on all three classes.

6 Discussion

This thesis aimed to present a kernel-based SVM predictive framework to classify AD clinical groups in elderly aging subjects at the risk of AD. The study uses volumetric MR baseline and longitudinal DZNE DELCODE cohort. In this thesis, we studied binary classification problem, CN vs. MCI, and a multiclass classification problem, CN vs. SCDs vs. MCIs, for the baseline & longitudinal data. The presented image-based predictive framework uses two flavors of the SVM model 1) standard SVM model and 2) a weighted SVM model which specifies the weights for each data point in every class. One advantage of using weighted SVM is to handle the class imbalance. Furthermore, the framework employs a linear kernel to estimate the similarity between voxels of each subject. Earlier studies [(KLÖPPEL et al., 2008; MESROB et al., 2009)] have pointed out the use of linear kernel in the context of the SVM neuroimaging framework performs slightly better than non-linear kernels. Moreover, significant benefits of the linear kernel are 1) it is relatively easy to implement with no hyperparameters parameterization and 2) mapping high dimensional imaging data to a lower-dimensional subspace. Thus, reducing the complexity of the model.

6.1 Baseline Models

6.1.1 Classification of CN vs. MCI

In classifying subjects CN from MCI, we observed that in the case of cross-validation, the weighted SVM performance was slightly better than the standard SVM model due to the weight assignment data sample according to the unbalanced class frequency. to each (see Table 5.1). For the unseen data pre-

diction using the test, the standard SVM and weighted SVM performed the same with a performance score of 75%. Earlier studies [(CAO et al., 2017; LI et al., 2015)] have shown similar performance while discriminating cognitive normal and cognitively impaired subjects. In the study, proposed by [LI et al. (2015)] the baseline method using SVM for classifying CN vs. MCI was estimated to be 72.1% and, in comparison to our method, achieved slightly higher performance. Overall, we see a minor improvement in the performance in the case of weighted SVM.

6.1.2 Classification of CN vs. SCD vs. MCI

The cross-validation scores in classifying subjects from CN vs. SCD vs. MCI was comparatively lower than that of binary classification of CN vs. MCI (see Table 5.3). Since multi-class classification is more challenging since more classes have to be consistently separated using structural imaging features. In particular, the MRI-based separation of CN and SCD might be poor since early stages do not show strong macro-structural changes compared to MCI. Furthermore, other neuroimaging features such as CSF biomarkers, demographics features, CSF, WM tissue types might be used in the future to improve the multi-class classification.

Additionally, we observe that accuracy scores are relatively high for both the classifiers, resulting from the imbalanced class distribution compared with the binary classification problem. Finally, using the untouched data to test the model's generalizability, the estimated performance was similar to that of the cross-validation score. However, similar to CV scores, the weighted SVM seems to perform slightly better than the standard SVM.

6.2 Longitudinal Models

6.2.1 Classification of CN vs. MCI

We can see the performance of the classification models for longitudinal MRI data in Table 5.5. Here, we have obtained an accuracy of 75% and 77% for the standard and weighted SVM, respectively. We observed an improvement in the accuracy scores for both models compared to baseline MRI data analysis. However, accuracy can sometimes be misleading when the dataset is imbalanced. Therefore, we further assessed the performance with F1 scores. As

we show in Table 5.5, the F1 score for the standard SVM model is 65%, while for the weighted SVM, it improved to 69%, indicating a decline in the models' performance compared with a baseline study using only baseline MRI features. We have computed AUC scores for further assessment, which define the model's performance on discriminating the target classes. The AUC for standard SVM was 70% while it was 72% for weighted SVM. We observe here a slight improvement with assigned weights to each class instance.

Furthermore, the performance on a test sample attained an increment in performance compared to baseline MRI data analysis. As we can see in Table 5.6, standard and weighted SVM performed similarly and produced an accuracy of 82% while an F1 score of 81%. Additionally, Figure 5.4 suggests an overlap of ROC curves for our classification algorithms with a similar AUC score of 82%. Moreover, we have computed the optimum thresholds for the presented models. We attained an optimum threshold for standard SVM as 0.39, whereas we observed a slight shift in the optimum threshold for weighted SVM with 0.49. Compared to the baseline models, the longitudinal models have performed slightly better in classifying cognitive normal from cognitively impaired.

6.2.2 Classification of CN vs. SCD vs. MCI

The performance of standard SVM and weighted SVM based on longitudinal MRI data in classifying CN vs. SCD vs. MCI was estimated with an accuracy score of 55%, F1 score of 48%, and an AUC score of 66% and accuracy score of 55%, F1 score of 48%, and AUC score of 66% respectively (see Table 5.7).

The test sample performance for the standard SVM was estimated to be 47% accuracy and 46% F1 score while weighted SVM outperformed standard SVM with an accuracy score of 50% and F1 score of 47%. Additionally, we were able to improve the accuracy to 50% for weighted SVM, it was 48% in the case of baseline MRI data. The performance on the test same was similar to that of CV scores. Overall, the longitudinal model seems to perform slightly better than the baseline model.

7

Conclusions and Future Work

This thesis aimed to build a classification model for baseline and longitudinal MRI data analysis of the DZNE DELCODE cohort. The primary goal of this work was to detect the different clinical AD groups. We first developed classification models for baseline structural neuroimaging data, which served as a baseline approach for this study. The classification algorithms were designed to address binary and multi-class classification tasks that separate individual patient's diagnostic group membership based on their structural brain pattern. The binary classification was done for healthy subjects and subjects with MCI. Furthermore we performend multiclass-classification among these two groups and a third group showing SCD. We have used the standard SVM model in two different settings. First, we have designed a linear SVM model with default parameters called base SVM. Secondly, we included weights for every data instance in the dataset while aiming to efficiently handle the class imbalance in the dataset. In the following subsections, we describe the general conclusions of this work and directions for future work.

The key question of the thesis was whether longitudinal neuroimaging data does offer potential for improved MR-based prediction and classification of diagnostic stages. The general performance of the classification models for longitudinal MRI data analysis tended to improve for both binary and multi-class classification compared to a model which only uses cross-sectional (i.e. baseline) MRI data. In addition, for each study, we observed that weighted SVM outperformed the standard SVM model therefore, we can conclude that class imbalance might be degrading the performance of the applied classification algorithms. Furthermore, we observed that binary classification performed better than multi-class. This was partially expected since multi-class classification is harder since more classes have to be consistently separated using structural imaging features. In particular, the MRI-based separation of

CN and SCD might be poor since early stages do not show strong macrostructural changes compared to MCI. Other neuroimaging features might be used in the future to improve the multi-class classification.

7.1 Limitations and Directions for future work

In this thesis, we have incorporated only the linear kernel to handle the high-dimensional MR feature however, SVM is a versatile machine learning algorithm that can be employed with different kernel functions such as polynomial with a varied degree, radial basis function kernel, or sigmoid kernel. Additionally, one might be interested in defining a pre-computed kernel to suit their specific task. The choices for machine learning algorithms can also be vast, including CNN[JAIN et al. (2019)], Random Forest, Multiple Kernel Learning, or Gaussian Process Regression [JOLLANS et al. (2019)]. The neuroimaging modalities can also be explored for classification and progression of AD or any neurological disorders [SANDOR et al. (1988), NORDBERG et al. (2010), DING et al. (2019)]. Moreover, other tissue volume segments i.e., WM and CSF, can be included for more extensive analysis of alteration in brain structure due to any neurological disorder.

Medical data is prone to an imbalance in class distribution, for instance, any rare disease will always have fewer positive cases than total tested subjects. Therefore the future work for this study might involve exploring the statistical resampling methods for balancing the dataset. Two fundamental approaches for balancing the dataset include oversampling and undersampling. The resampling could be done by randomly copying the data instances from the minority class or randomly deleting the samples from the majority class. These are some available fundamental resampling methods and do not follow any heuristics to address the problem. However, one could also use a more sophisticated method like Synthetic Minority Oversampling Technique (SMOTE), which generates the synthetic samples in the minority class using the K-nearest neighbors methodology. Furthermore, another extension to this work might involve including additional features to improve the performance of a classifier [FAN et al. (2007); LI et al. (2015)].

A

Abbreviations and Notations

Acronym	Meaning
AD	Alzheimer's Disease
ADNI	Alzheimer's Disease Neuroimaging Initiative
ADR	Alzheimer's Disease Relative
AUC	Area Under the Curve
AUROC	Area Under the Receiver Operating Characteristics
CAT	Computational Anatomy Toolbox
CNN	Convolutional Neural Networks
CN	Cognitive Normal
CSF	Cerebrospinal Fluid
CT	Computed Tomography
DARTEL	Diffeomorphic Anatomical Registration Through Exponentiated Lie algebra
DZNE	German Center for Neurodegenerative Diseases
DELCODE	DZNE-Longitudinal Cognitive Impairment and Dementia Study
fMRI	functional Magnetic Resonance Imaging
FPR	False Positive Rate
FWHM	Full Width at Half Maxima
GM	Grey Matter
ICV	Intracranial Volume
MCI	Mild Cognitive Impairment
MRI	Magnetic Resonance Imaging
OvR	One-vs-Rest
PET	Positron Emission Tomography
RF	Radio Frequency
ROC	Receiver Operating Characteristic
ROI	Region of Interest

Acronym	Meaning
RVM	Relevance Vector Machine
SCD	Subjective Cognitive Decline
sMRI	structural Magnetic Resonance Imaging
SMOTE	Synthetic Minority Oversampling Technique
SVM	Support Vector Machines
TBM	Tensor-based Morphometry
TE	Time of Echo
TPR	True Positive Rate
TR	Repetition Time
VBM	Voxel-based Morphometry
WM	White Matter

B

List of Figures

List of Tables

D
Bibliography

[ASHBURNER 2007] J. Ashburner. **A fast diffeomorphic image registration algorithm**. Neuroimage, Vol. 38(1):95–113, 2007.

[BALL et al. 1985] M. Ball, V. Hachinski, A. Fox, A. Kirshen, M. Fisman, W. Blume, V. Kral, H. Fox und H. Merskey. **A NEW DEFINITION OF ALZHEIMER'S DISEASE: A HIPPOCAMPAL DEMENTIA**. The Lancet, Vol. 325(8419):14–16, 1985. Originally published as Volume 1, Issue 8419.

[BASAIA et al. 2019] S. Basaia, F. Agosta, L. Wagner, E. Canu, G. Magnani, R. Santangelo, M. Filippi, A. D. N. Initiative et al. **Automated classification of Alzheimer's disease and mild cognitive impairment using a single MRI and deep neural networks**. NeuroImage: Clinical, Vol. 21:101645, 2019.

[BIRD 2008] T. D. Bird. **Genetic aspects of Alzheimer disease**. Genetics in Medicine, Vol. 10(4):231–239, 2008.

[BRAAK und BRAAK 1995] H. Braak und E. Braak. **Staging of Alzheimer's disease-related neurofibrillary changes**. Neurobiology of aging, Vol. 16(3):271–278, 1995.

[BRAUN 2008] M. M. Braun. **Neurological disorders.** 2008.

[BROOKMEYER et al. 2007] R. Brookmeyer, E. Johnson, K. Ziegler-Graham und H. M. Arrighi. **Forecasting the global burden of Alzheimer's disease**. Alzheimer's Dementia, Vol. 3(3):186–191, 2007.

[CAO et al. 2017] P. Cao, X. Liu, J. Yang, D. Zhao, M. Huang, J. Zhang und O. Zaiane. **Nonlinearity-aware based dimensionality reduction and over-**

sampling for AD/MCI classification from MRI measures. Computers in biology and medicine, Vol. 91:21–37, 2017.

[CHUPIN et al. 2009] M. Chupin, E. Gérardin, R. Cuingnet, C. Boutet, L. Lemieux, S. Lehéricy, H. Benali, L. Garnero und O. Colliot. **Fully automatic hippocampus segmentation and classification in Alzheimer's disease and mild cognitive impairment applied on data from ADNI**. Hippocampus, Vol. 19(6):579–587, 2009.

[COLLIOT et al. 2008] O. Colliot, G. Chételat, M. Chupin, B. Desgranges, B. Magnin, H. Benali, B. Dubois, L. Garnero, F. Eustache und S. Lehéricy. **Discrimination between Alzheimer disease, mild cognitive impairment, and normal aging by using automated segmentation of the hippocampus**. Radiology, Vol. 248(1):194–201, 2008.

[CORTES und VAPNIK 1995] C. Cortes und V. Vapnik. **Support-vector networks**. Machine learning, Vol. 20(3):273–297, 1995.

[DAVATZIKOS et al. 2008] C. Davatzikos, Y. Fan, X. Wu, D. Shen und S. M. Resnick. **Detection of prodromal Alzheimer's disease via pattern classification of magnetic resonance imaging**. Neurobiology of aging, Vol. 29(4):514–523, 2008.

[DE LEON et al. 1989] M. De Leon, A. George, L. Stylopoulos, G. Smith und D. Miller. **EARLY MARKER FOR ALZHEIMER'S DISEASE: THE ATROPHIC HIPPOCAMPUS**. The Lancet, Vol. 334(8664):672–673, 1989. Originally published as Volume 2, Issue 8664.

[DE LEON et al. 1993] M. De Leon, J. Golomb, A. George, A. Convit, C. Tarshish, T. McRae, S. De Santi, G. Smith, S. Ferris und M. Noz. **The radiologic prediction of Alzheimer disease: the atrophic hippocampal formation.** American Journal of Neuroradiology, Vol. 14(4):897–906, 1993.

[DEKOSKY et al. 2002] S. T. DeKosky, M. D. Ikonomovic, S. D. Styren, L. Beckett, S. Wisniewski, D. A. Bennett, E. J. Cochran, J. H. Kordower und E. J. Mufson. **Upregulation of choline acetyltransferase activity in hippocampus and frontal cortex of elderly subjects with mild cognitive impairment**. Annals of Neurology: Official Journal of the American Neurological Association and the Child Neurology Society, Vol. 51(2):145–155, 2002.

[DING et al. 2019] Y. Ding, J. H. Sohn, M. G. Kawczynski, H. Trivedi, R. Harnish, N. W. Jenkins, D. Lituiev, T. P. Copeland, M. S. Aboian, C. M. Aparici,

S. C. Behr, R. R. Flavell, S. Y. Huang, K. A. Zalocusky, L. Nardo, Y. Seo, R. A. Hawkins, M. H. Pampaloni, D. Hadley und B. L. Franc. **A deep learning model to predict a diagnosis of Alzheimer disease by using 18 F-FDG PET of the brain**. Radiology, Vol. 290:456–464, 2019.

[DU et al. 2001] A. Du, N. Schuff, D. Amend, M. Laakso, Y. Hsu, W. Jagust, K. Yaffe, J. Kramer, B. Reed, D. Norman et al. **Magnetic resonance imaging of the entorhinal cortex and hippocampus in mild cognitive impairment and Alzheimer's disease**. Journal of Neurology, Neurosurgery & Psychiatry, Vol. 71(4):441–447, 2001.

[DUBOIS et al. 2016] B. Dubois, H. Hampel, H. H. Feldman, P. Scheltens, P. Aisen, S. Andrieu, H. Bakardjian, H. Benali, L. Bertram, K. Blennow et al. **Preclinical Alzheimer's disease: definition, natural history, and diagnostic criteria**. Alzheimer's & Dementia, Vol. 12(3):292–323, 2016.

[DUNN et al. 2021] B. Dunn, P. Stein und P. Cavazzoni. **Approval of aducanumab for Alzheimer disease—the FDA's perspective**. JAMA internal medicine, Vol. 181(10):1276–1278, 2021.

[ERKINJUNTTI et al. 1993] T. Erkinjuntti, D. H. Lee, F. Gao, R. Steenhuis, M. Eliasziw, R. Fry, H. Merskey und V. C. Hachinski. **Temporal lobe atrophy on magnetic resonance imaging in the diagnosis of early Alzheimer's disease**. Archives of Neurology, Vol. 50(3):305–310, 1993.

[FAN et al. 2008] Y. Fan, N. Batmanghelich, C. M. Clark und C. Davatzikos. **Spatial patterns of brain atrophy in MCI patients, identified via high-dimensional pattern classification, predict subsequent cognitive decline**. NeuroImage, Vol. 39(4):1731–1743, 2008a.

[FAN et al. 2007] Y. Fan, H. Rao, H. Hurt, J. Giannetta, M. Korczykowski, D. Shera, B. B. Avants, J. C. Gee, J. Wang und D. Shen. **Multivariate examination of brain abnormality using both structural and functional MRI**. NeuroImage, Vol. 36(4):1189–1199, 2007.

[FAN et al. 2008] Y. Fan, S. M. Resnick, X. Wu und C. Davatzikos. **Structural and functional biomarkers of prodromal Alzheimer's disease: A high-dimensional pattern classification study**. NeuroImage, Vol. 41(2):277–285, 2008b.

[FLEISHER et al. 2005] A. S. Fleisher, W. S. Houston, L. T. Eyler, S. Frye, C. Jenkins, L. J. Thal und M. W. Bondi. **Identification of Alzheimer disease**

risk by functional magnetic resonance imaging. Archives of Neurology, Vol. 62(12):1881–1888, 2005.

[FOSTER et al. 2011] P. Foster, K. Rosenblatt und R. Kuljiš. **Exercise-Induced Cognitive Plasticity, Implications for Mild Cognitive Impairment and Alzheimer's Disease**. Frontiers in neurology, Vol. 2:28, 2011.

[FOX et al. 1999] N. Fox, R. Scahill, W. Crum und M. Rossor. **Correlation between rates of brain atrophy and cognitive decline in AD**. Neurology, Vol. 52(8):1687–1687, 1999.

[FRACKOWIAK 2004] R. S. Frackowiak. **Human brain function**. Elsevier, 2004.

[FRANKE und GASER 2012] K. Franke und C. Gaser. **Longitudinal changes in individual BrainAGE in healthy aging, mild cognitive impairment, and Alzheimer's disease**. GeroPsych, 2012.

[FRANKE und GASER 2014] K. Franke und C. Gaser. **Dementia classification based on brain age estimation**. In: Proc MICCAI Workshop Challenge on Computer-Aided Diagnosis of Dementia Based on Structural MRI Data, 2014, pp. 48–54.

[FRANKE et al. 2010] K. Franke, G. Ziegler, S. Klöppel, C. Gaser, A. D. N. Initiative et al. **Estimating the age of healthy subjects from T1-weighted MRI scans using kernel methods: exploring the influence of various parameters**. Neuroimage, Vol. 50(3):883–892, 2010.

[FRISONI et al. 2010] G. B. Frisoni, N. C. Fox, C. R. Jack, P. Scheltens und P. M. Thompson. **The clinical use of structural MRI in Alzheimer disease**. Nature Reviews Neurology, Vol. 6(2):67–77, 2010.

[GASER et al. 2016] C. Gaser, R. Dahnke et al. **CAT-a computational anatomy toolbox for the analysis of structural MRI data**. Hbm, Vol. 2016:336–348, 2016.

[GAUGLER et al. 2019] J. Gaugler, B. James, T. Johnson, A. Marin und J. Weuve. **2019 Alzheimer's disease facts and figures**. Alzheimers & Dementia, Vol. 15(3):321–387, 2019.

[GAUTHIER et al. 2006] S. Gauthier, B. Reisberg, M. Zaudig, R. C. Petersen, K. Ritchie, K. Broich, S. Belleville, H. Brodaty, D. Bennett, H. Chertkow, J. L. Cummings, M. de Leon, H. Feldman, M. Ganguli, H. Hampel, P. Scheltens, M. C. Tierney, P. Whitehouse und B. Winblad. **Mild cognitive impairment**. The Lancet, Vol. 367(9518):1262–1270, 2006.

[GERARDIN et al. 2009] E. Gerardin, G. Chételat, M. Chupin, R. Cuingnet, B. Desgranges, H.-S. Kim, M. Niethammer, B. Dubois, S. Lehéricy, L. Garnero et al. **Multidimensional classification of hippocampal shape features discriminates Alzheimer's disease and mild cognitive impairment from normal aging**. Neuroimage, Vol. 47(4):1476–1486, 2009.

[GOSCHE et al. 2002] K. Gosche, J. Mortimer, C. Smith, W. Markesbery und D. Snowdon. **Hippocampal volume as an index of Alzheimer neuropathology: findings from the Nun Study**. Neurology, Vol. 58(10):1476–1482, 2002.

[HANDELMAN et al. 2019] G. S. Handelman, H. K. Kok, R. V. Chandra, A. H. Razavi, S. Huang, M. Brooks, M. J. Lee und H. Asadi. **Peering into the black box of artificial intelligence: evaluation metrics of machine learning methods**. American Journal of Roentgenology, Vol. 212(1):38–43, 2019.

[HANE et al. 2017] F. T. Hane, M. Robinson, B. Y. Lee, O. Bai, Z. Leonenko und M. S. Albert. **Recent Progress in Alzheimer's Disease Research, Part 3: Diagnosis and Treatment**. Journal of Alzheimer's Disease, Vol. 57:645–665, 2017a. 3.

[HANE et al. 2017] F. T. Hane, M. Robinson, B. Y. Lee, O. Bai, Z. Leonenko und M. S. Albert. **Recent progress in Alzheimer's disease research, part 3: diagnosis and treatment**. Journal of Alzheimer's Disease, Vol. 57(3):645–665, 2017b.

[HARDIMAN et al. 2011] O. Hardiman, C. P. Doherty, M. Elamin und P. Bede. **Neurodegenerative disorders**. Springer, 2011.

[HENNEMAN et al. 2009] W. Henneman, J. Sluimer, J. Barnes, W. Van Der Flier, I. Sluimer, N. Fox, P. Scheltens, H. Vrenken und F. Barkhof. **Hippocampal atrophy rates in Alzheimer disease: added value over whole brain volume measures**. Neurology, Vol. 72(11):999–1007, 2009.

[HONG und CHO 2008] J.-H. Hong und S.-B. Cho. **A probabilistic multi-class strategy of one-vs.-rest support vector machines for cancer classification**. Neurocomputing, Vol. 71(16-18):3275–3281, 2008.

[HUANG et al. 2010] S. Huang, J. Li, L. Sun, J. Ye, A. Fleisher, T. Wu, K. Chen und E. Reiman. **Learning brain connectivity of Alzheimer's disease by sparse inverse covariance estimation**. NeuroImage, Vol. 50(3):935–949, 2010.

[JACK et al. 2008] C. Jack, S. D. Weigand, M. M. Shiung, S. A. Przybelski, P. C. O'Brien, J. L. Gunter, D. S. Knopman, B. F. Boeve, G. E. Smith und R. C. Petersen. **Atrophy rates accelerate in amnestic mild cognitive impairment**. Neurology, Vol. 70(19 Part 2):1740–1752, 2008.

[JACK et al. 2018] C. R. Jack, D. A. Bennett, K. Blennow, M. C. Carrillo, B. Dunn, S. B. Haeberlein, D. M. Holtzman, W. Jagust, F. Jessen, J. Karlawish, E. Liu, J. L. Molinuevo, T. Montine, C. Phelps, K. P. Rankin, C. C. Rowe, P. Scheltens, E. Siemers, H. M. Snyder, R. Sperling, C. Elliott, E. Masliah, L. Ryan und N. Silverberg. **NIA-AA Research Framework: Toward a biological definition of Alzheimer's disease**. Alzheimer's Dementia, Vol. 14(4):535–562, 2018.

[JACK et al. 2013] C. R. Jack, D. S. Knopman, W. J. Jagust, R. C. Petersen, M. W. Weiner, P. S. Aisen, L. M. Shaw, P. Vemuri, H. J. Wiste, S. D. Weigand, T. G. Lesnick, V. S. Pankratz, M. C. Donohue und J. Q. Trojanowski. **Tracking pathophysiological processes in Alzheimer's disease: an updated hypothetical model of dynamic biomarkers**. The Lancet Neurology, Vol. 12(2):207–216, 2013.

[JACK JR et al. 2010] C. R. Jack Jr, H. J. Wiste, P. Vemuri, S. D. Weigand, M. L. Senjem, G. Zeng, M. A. Bernstein, J. L. Gunter, V. S. Pankratz, P. S. Aisen et al. **Brain beta-amyloid measures and magnetic resonance imaging atrophy both predict time-to-progression from mild cognitive impairment to Alzheimer's disease**. Brain, Vol. 133(11):3336–3348, 2010.

[JAIN et al. 2019] R. Jain, N. Jain, A. Aggarwal und D. J. Hemanth. **Convolutional neural network based Alzheimer's disease classification from magnetic resonance brain images**. Cognitive Systems Research, Vol. 57:147–159, 2019.

[JESSEN et al. 2014] F. Jessen, R. E. Amariglio, M. Van Boxtel, M. Breteler, M. Ceccaldi, G. Chételat, B. Dubois, C. Dufouil, K. A. Ellis, W. M. Van Der Flier et al. **A conceptual framework for research on subjective cognitive decline in preclinical Alzheimer's disease**. Alzheimer's & dementia, Vol. 10(6):844–852, 2014.

[JOLLANS et al. 2019] L. Jollans, R. Boyle, E. Artiges, T. Banaschewski, S. Desrivières, A. Grigis, J.-L. Martinot, T. Paus, M. N. Smolka, H. Walter, G. Schumann, H. Garavan und R. Whelan. **Quantifying performance of machine learning methods for neuroimaging data**. NeuroImage, Vol. 199:351–365, 2019.

[KALES et al. 2015] H. C. Kales, L. N. Gitlin und C. G. Lyketsos. **Assessment and management of behavioral and psychological symptoms of dementia**. Bmj, Vol. 350, 2015.

[KAUWE et al. 2010] J. S. Kauwe, C. Cruchaga, S. Bertelsen, K. Mayo, W. Latu, P. Nowotny, A. L. Hinrichs, A. M. Fagan, D. M. Holtzman, A. M. Goate et al. **Validating predicted biological effects of Alzheimer's disease associated SNPs using CSF biomarker levels**. Journal of Alzheimer's Disease, Vol. 21(3):833–842, 2010.

[KELLER und ROBERTS 2008] S. S. Keller und N. Roberts. **Voxel-based morphometry of temporal lobe epilepsy: an introduction and review of the literature**. Epilepsia, Vol. 49(5):741–757, 2008.

[KLÖPPEL et al. 2012] S. Klöppel, A. Abdulkadir, C. R. Jack Jr, N. Koutsouleris, J. Mourão-Miranda und P. Vemuri. **Diagnostic neuroimaging across diseases**. Neuroimage, Vol. 61(2):457–463, 2012.

[KLÖPPEL et al. 2008] S. Klöppel, C. M. Stonnington, C. Chu, B. Draganski, R. I. Scahill, J. D. Rohrer, N. C. Fox, C. R. Jack Jr, J. Ashburner und R. S. Frackowiak. **Automatic classification of MR scans in Alzheimer's disease**. Brain, Vol. 131(3):681–689, 2008.

[KLÖPPEL et al. 2008] S. Klöppel, C. M. Stonnington, C. Chu, B. Draganski, R. I. Scahill, J. D. Rohrer, N. C. Fox, J. Jack, Clifford R., J. Ashburner und R. S. J. Frackowiak. **Automatic classification of MR scans in Alzheimer's disease**. Brain, Vol. 131(3):681–689, 2008.

[LAAKSO et al. 2000] M. P. Laakso, G. B. Frisoni, M. Könönen, M. Mikkonen, A. Beltramello, C. Geroldi, A. Bianchetti, M. Trabucchi, H. Soininen und H. J. Aronen. **Hippocampus and entorhinal cortex in frontotemporal dementia and Alzheimer's disease: a morphometric MRI study**. Biological psychiatry, Vol. 47(12):1056–1063, 2000.

[LAO et al. 2004] Z. Lao, D. Shen, Z. Xue, B. Karacali, S. M. Resnick und C. Davatzikos. **Morphological classification of brains via high-dimensional shape transformations and machine learning methods**. Neuroimage, Vol. 21(1):46–57, 2004a.

[LAO et al. 2004] Z. Lao, D. Shen, Z. Xue, B. Karacali, S. M. Resnick und C. Davatzikos. **Morphological classification of brains via high-dimensional shape transformations and machine learning methods**. NeuroImage, Vol. 21(1):46–57, 2004b.

[LI et al. 2018] F. Li, M. Liu, A. D. N. Initiative et al. **Alzheimer's disease diagnosis based on multiple cluster dense convolutional networks**. Computerized Medical Imaging and Graphics, Vol. 70:101–110, 2018.

[LI et al. 2015] F. Li, L. Tran, K.-H. Thung, S. Ji, D. Shen und J. Li. **A robust deep model for improved classification of AD/MCI patients**. IEEE journal of biomedical and health informatics, Vol. 19(5):1610–1616, 2015.

[LI et al. 2019] H. Li, M. Habes, D. A. Wolk, Y. Fan, A. D. N. Initiative et al. **A deep learning model for early prediction of Alzheimer's disease dementia based on hippocampal magnetic resonance imaging data**. Alzheimer's & Dementia, Vol. 15(8):1059–1070, 2019.

[LUO et al. 2017] S. Luo, X. Li und J. Li. **Automatic Alzheimer's disease recognition from MRI data using deep learning method**. Journal of Applied Mathematics and Physics, Vol. 5(9):1892–1898, 2017.

[MA und GUO 2014] Y. Ma und G. Guo. **Support vector machines applications**, Vol. 649. Springer, 2014.

[MAGALINGAM et al. 2018] K. B. Magalingam, A. Radhakrishnan, N. S. Ping und N. Haleagrahara. **Current concepts of neurodegenerative mechanisms in Alzheimer's disease**. BioMed research international, Vol. 2018, 2018.

[MAGNIN et al. 2009] B. Magnin, L. Mesrob, S. Kinkingnéhun, M. Pélégrini-Issac, O. Colliot, M. Sarazin, B. Dubois, S. Lehéricy und H. Benali. **Support vector machine-based classification of Alzheimer's disease from whole-brain anatomical MRI**. Neuroradiology, Vol. 51(2):73–83, 2009.

[MCROBBIE et al. 2017] D. W. McRobbie, E. A. Moore, M. J. Graves und M. R. Prince. **MRI from Picture to Proton**. Cambridge university press, 2017.

[MESROB et al. 2009] L. Mesrob, B. Magnin, O. Colliot, M. Sarazin, V. Hahn-Barma, B. Dubois, P. Gallinari, S. Lehéricy, S. Kinkingnéhun und H. Benali. **Identification of atrophy patterns in Alzheimer's disease based on SVM feature selection and anatomical par-cellation**. Annals of the BMVA Vol, Vol. 2009(7):1–9, 2009.

[MISRA et al. 2009] C. Misra, Y. Fan und C. Davatzikos. **Baseline and longitudinal patterns of brain atrophy in MCI patients, and their use in prediction of short-term conversion to AD: results from ADNI**. Neuroimage, Vol. 44(4):1415–1422, 2009.

[MORMINO et al. 2009] E. Mormino, J. Kluth, C. Madison, G. Rabinovici, S. Baker, B. Miller, R. Koeppe, C. Mathis, M. Weiner, W. Jagust et al. **Episodic memory loss is related to hippocampal-mediated β-amyloid deposition in elderly subjects**. Brain, Vol. 132(5):1310–1323, 2009.

[NARKHEDE 2018] S. Narkhede. **Understanding auc-roc curve**. Towards Data Science, Vol. 26(1):220–227, 2018.

[NORDBERG et al. 2010] A. Nordberg, J. O. Rinne, A. Kadir und B. Långström. **The use of PET in Alzheimer disease**. Nature Reviews Neurology, Vol. 6(2):78–87, 2010.

[NOWINSKI 2011] W. L. Nowinski. **Introduction to brain anatomy**. In: Biomechanics of the Brain, pp. 5–40. 2011. Springer.

[OMBAO et al. 2016] H. Ombao, M. Lindquist, W. Thompson und J. Aston. **Handbook of neuroimaging data analysis**. Chapman and Hall/CRC, 2016.

[ORGANIZATION. 2006] W. H. Organization. **Neurological disorders : public health challenges**. World Health Organization Geneva, 2006.

[PEDREGOSA et al. 2011] F. Pedregosa, G. Varoquaux, A. Gramfort, V. Michel, B. Thirion, O. Grisel, M. Blondel, P. Prettenhofer, R. Weiss, V. Dubourg, J. Vanderplas, A. Passos, D. Cournapeau, M. Brucher, M. Perrot und E. Duchesnay. **Scikit-learn: Machine Learning in Python**. Journal of Machine Learning Research, Vol. 12:2825–2830, 2011.

[PINI et al. 2016] L. Pini, M. Pievani, M. Bocchetta, D. Altomare, P. Bosco, E. Cavedo, S. Galluzzi, M. Marizzoni und G. B. Frisoni. **Brain atrophy in Alzheimer's disease and aging**. Ageing research reviews, Vol. 30:25–48, 2016.

[QIU et al. 2017] R. G. Qiu, J. L. Qiu und Y. Badr. **Predictive modeling of the severity/progression of alzheimer's diseases**. In: 2017 International Conference on Grey Systems and Intelligent Services (GSIS), pp. 400–403. 2017, IEEE.

[QUERBES et al. 2009] O. Querbes, F. Aubry, J. Pariente, J.-A. Lotterie, J.-F. Démonet, V. Duret, M. Puel, I. Berry, J.-C. Fort, P. Celsis et al. **Early diagnosis of Alzheimer's disease using cortical thickness: impact of cognitive reserve**. Brain, Vol. 132(8):2036–2047, 2009.

[RASKIN et al. 2015] J. Raskin, J. Cummings, J. Hardy, K. Schuh und R. A Dean. **Neurobiology of Alzheimer's disease: integrated molecular, physiological, anatomical, biomarker, and cognitive dimensions**. Current Alzheimer Research, Vol. 12(8):712–722, 2015.

[RISACHER und SAYKIN 2011] S. L. Risacher und A. J. Saykin. **Neuroimaging of Alzheimer's disease, mild cognitive impairment, and other dementias**. In: Brain Imaging in Behavioral Medicine and Clinical Neuroscience, pp. 309–339. 2011. Springer.

[RISACHER und SAYKIN 2013] S. L. Risacher und A. J. Saykin. **Neuroimaging and other biomarkers for Alzheimer's disease: the changing landscape of early detection**. Annual review of clinical psychology, Vol. 9:621–648, 2013.

[RISACHER et al. 2009] S. L. Risacher, A. J. Saykin, J. D. Wes, L. Shen, H. A. Firpi und B. C. McDonald. **Baseline MRI predictors of conversion from MCI to probable AD in the ADNI cohort**. Current Alzheimer Research, Vol. 6(4):347–361, 2009.

[RISACHER et al. 2010] S. L. Risacher, L. Shen, J. D. West, S. Kim, B. C. McDonald, L. A. Beckett, D. J. Harvey, C. R. Jack Jr, M. W. Weiner, A. J. Saykin et al. **Longitudinal MRI atrophy biomarkers: relationship to conversion in the ADNI cohort**. Neurobiology of aging, Vol. 31(8):1401–1418, 2010.

[ROSEN et al. 2002] H. J. Rosen, M. L. Gorno-Tempini, W. Goldman, R. Perry, N. Schuff, M. Weiner, R. Feiwell, J. Kramer und B. L. Miller. **Patterns of brain atrophy in frontotemporal dementia and semantic dementia**. Neurology, Vol. 58(2):198–208, 2002.

[RUSINEK et al. 2003] H. Rusinek, S. De Santi, D. Frid, W.-H. Tsui, C. Y. Tarshish, A. Convit und M. J. de Leon. **Regional brain atrophy rate predicts future cognitive decline: 6-year longitudinal MR imaging study of normal aging**. Radiology, Vol. 229(3):691–696, 2003.

[SANDOR et al. 1988] T. Sandor, M. Albert, J. Stafford und S. Harpley. **Use of computerized CT analysis to discriminate between Alzheimer patients and normal control subjects.** American Journal of Neuroradiology, Vol. 9(6):1181–1187, 1988.

[SAVVA et al. 2009] G. M. Savva, S. B. Wharton, P. G. Ince, G. Forster, F. E. Matthews und C. Brayne. **Age, neuropathology, and dementia**. New England Journal of Medicine, Vol. 360(22):2302–2309, 2009.

[SCHOTT et al. 2005] J. Schott, S. Price, C. Frost, J. Whitwell, M. Rossor und N. Fox. **Measuring atrophy in Alzheimer disease: a serial MRI study over 6 and 12 months**. Neurology, Vol. 65(1):119–124, 2005.

[SCHÖLKOPF et al. 2001] B. Schölkopf, J. C. Platt, J. Shawe-Taylor, A. J. Smola und R. C. Williamson. **Estimating the Support of a High-Dimensional Distribution**. Neural Computation, Vol. 13(7):1443–1471, 2001.

[SHARMA et al. 2021] G. Sharma, A. Vijayvargiya und R. Kumar. **Comparative Assessment among Different Convolutional Neural Network Architectures for Alzheimer's Disease Detection**. In: 2021 IEEE 8th Uttar Pradesh Section International Conference on Electrical, Electronics and Computer Engineering (UPCON), pp. 1–6. 2021, IEEE.

[SHAWE-TAYLOR et al. 2004] J. Shawe-Taylor, N. Cristianini et al. **Kernel methods for pattern analysis**. Cambridge university press, 2004.

[SHIN et al. 2005] I.-S. Shin, M. Carter, D. Masterman, L. Fairbanks und J. L. Cummings. **Neuropsychiatric symptoms and quality of life in Alzheimer disease**. The American journal of geriatric psychiatry, Vol. 13(6):469–474, 2005.

[SMALE et al. 1995] G. Smale, N. R. Nichols, D. R. Brady, C. E. Finch und W. E. Horton Jr. **Evidence for apoptotic cell death in Alzheimer's disease**. Experimental neurology, Vol. 133(2):225–230, 1995.

[SQUIRE 2004] L. R. Squire. **Memory systems of the brain: a brief history and current perspective**. Neurobiology of learning and memory, Vol. 82(3):171–177, 2004.

[T. HASTIE 2008] J. F. T. Hastie, R. Tibshirani. **The Elements of Statistical Learning**. Springer, 2008.

[TEIPEL et al. 2007] S. J. Teipel, C. Born, M. Ewers, A. L. Bokde, M. F. Reiser, H.-J. Möller und H. Hampel. **Multivariate deformation-based analysis of brain atrophy to predict Alzheimer's disease in mild cognitive impairment**. Neuroimage, Vol. 38(1):13–24, 2007.

[TERRY et al. 1991] R. D. Terry, E. Masliah, D. P. Salmon, N. Butters, R. DeTeresa, R. Hill, L. A. Hansen und R. Katzman. **Physical basis of cognitive alterations in Alzheimer's disease: synapse loss is the major correlate of cognitive impairment**. Annals of Neurology: Official Journal of the American Neurological Association and the Child Neurology Society, Vol. 30(4):572–580, 1991.

[THAKARE und PAWAR 2016] P. Thakare und V. Pawar. **Alzheimer disease detection and tracking of Alzheimer patient**. In: 2016 International Conference on Inventive Computation Technologies (ICICT), Vol. 1, pp. 1–4. 2016, IEEE.

[TIPPING 1999] M. Tipping. **The Relevance Vector Machine**. In: S. Solla, T. Leen und K. Müller, Eds., Advances in Neural Information Processing Systems, Vol. 12. 1999, MIT Press.

[VAN DE POL et al. 2006] L. A. Van De Pol, A. Hensel, W. M. van der Flier, P. J. Visser, Y. A. Pijnenburg, F. Barkhof, H. J. Gertz und P. Scheltens. **Hippocampal atrophy on MRI in frontotemporal lobar degeneration and Alzheimer's disease**. Journal of Neurology, Neurosurgery & Psychiatry, Vol. 77(4):439–442, 2006.

[WEINER und KHACHATURIAN 2005] M. Weiner und Z. Khachaturian. **The use of MRI and PET for clinical diagnosis of dementia and investigation of cognitive impairment: a consensus report**. Alzheimer's Assoc Chicago, IL, Vol. 1:1–15, 2005.

[WEINTRAUB et al. 2012] D. Weintraub, N. Dietz, J. E. Duda, D. A. Wolk, J. Doshi, S. X. Xie, C. Davatzikos, C. M. Clark und A. Siderowf. **Alzheimer's disease pattern of brain atrophy predicts cognitive decline in Parkinson's disease**. Brain : a journal of neurology, Vol. 135(Pt 1):170–180, 2012. 22108576[pmid].

[WHITWELL 2009] J. L. Whitwell. **Voxel-based morphometry: an automated technique for assessing structural changes in the brain**. Journal of Neuroscience, Vol. 29(31):9661–9664, 2009.

[WHITWELL und JACK JR 2005] J. L. Whitwell und C. R. Jack Jr. **Comparisons between Alzheimer disease, frontotemporal lobar degeneration, and normal aging with brain mapping**. Topics in Magnetic Resonance Imaging, Vol. 16(6):409–425, 2005.

[WHITWELL und JOSEPHS 2007] J. L. Whitwell und K. A. Josephs. **Voxel-based morphometry and its application to movement disorders**. Parkinsonism & related disorders, Vol. 13:S406–S416, 2007.

[XUE et al. 2009] H. Xue, Q. Yang und S. Chen. **SVM: Support vector machines**. The top ten algorithms in data mining, Vol. 6(3):37–60, 2009.

[YIN XIA et al. 2015] S. yin Xia, Z. yang Xiong, Y. guo Luo und L. mei Dong. **A method to improve support vector machine based on distance to hyperplane**. Optik, Vol. 126(20):2405–2410, 2015.

[ZHANG et al. 2014] Y.-D. Zhang, S. Wang und Z. Dong. **Classification of Alzheimer disease based on structural magnetic resonance imaging by kernel support vector machine decision tree**. Progress In Electromagnetics Research, Vol. 144:171–184, 2014.

Declaration of Academic Integrity

I hereby declare that I have written the present work myself and did not use any sources or tools other than the ones indicated.

Datum: .....

(Signature)